Gone With the Headwind
Characterizing Erosion Using Lattice-Boltzmann Method

and its Implications in Planet Formation

Lukas Cedenblad

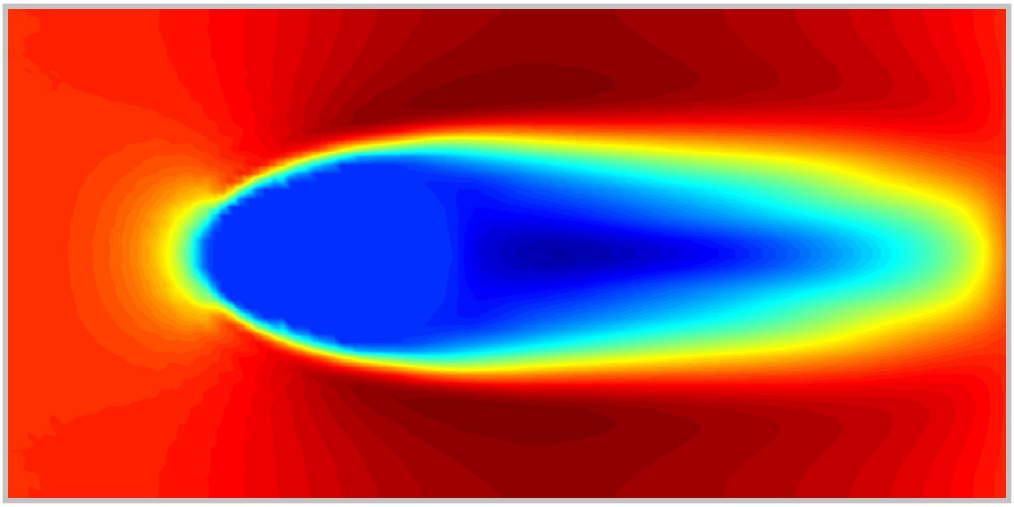

Department of physics, Fysikum
Master's thesis, 45hp
Programme: Computational physics
Supervisor: Dhrubaditya Mitra
February 5, 2019

Acknowledgements

My sincerest gratitude to my supervisor Dhrubaditya. You have the answer to almost everything and your energy and excitement with the project and physics in general has been very motivational during this time and inspirational to watch.
A huge thanks to all the people at nordita for the wonderful discussions and words of wisdom.
My friends who made me do other things than write on my thesis when i should have been writing on my thesis.
My family and girlfriend for your never ending love and support.

Abstract

Erosion has a long history in science and is used in many different fields today, for example in geology for coastal erosion and in oil industry for pipe erosion. It is very difficult to study erosion both analytically. Numerically it is difficult due to moving and shape-changing boundaries. Here we develop a numerical model in 3D using the Lattice-Boltzmann method, which is good at simulating complex moving boundaries, and erosion capabilities are implemented. Both laminar and turbulent flow can be modeled with this program. Using an experimentally derived model for the mass change due to erosion in clay and mud-type objects, one can derive equations predicting that the volume of a sphere should, due to erosion, scale as $V \sim -t^2$. This is also observed with simulations. The shapes of a double sphere with different orientations and a cube in laminar flow we find to have similar power law exponent P, $P = 2 \pm 0.1$. But a cube eroding in Re = 800 had no power law behaviour, meaning that the current analytical framework is incomplete. Possibility of a more general framework is presented for future research. Different Reynolds number also affected the power law behaviour and the shape change over time for the different solids.
Very little research has been made for erosion of planetesimals, but it has been argued that erosion can be relevant to their fate. Using the same erosion model, an equation of the erosion time is found for laminar flows and for a sphere. Simulation results find that the equation works within an order of magnitude for turbulent flows, a double sphere and a cube. This gives an estimate of the erosion time t^* of planetesimals to be $t^* \sim 1s$, given a size of radius equal to 10cm and 1km, an orbital eccentricity $e > 10^{-2}$ and a distance at r = 1 a.u. Implying that orbits for planetesimals with low eccentricity might be favoured.

Contents

Chapter 1

Symbols

1.1 Abbreviations

- LBE - Lattice-Boltzmann equations
- LBM - Lattice-Boltzmann method
- BGK - Bhatnagar, Gross and Krook
- NS - Navier-Stokes
- Ma - Mach number
- Re - Reynolds number
- Er - Erosion number

1.2 Variables

- f - distribution function.
- f_i - distribution function in the i:th direction.
- $f^{(\mathrm{eq})}, f^{(0)}$ - Equilibrium distribution function.
- μ - dynamic viscosity
- ν - kinematic viscosity.
- $\boldsymbol{\rho}$ - Density.
- $\boldsymbol{u}$ - Fluid velocity.
- $\boldsymbol{\xi}$ - Particle velocity.
- ξ_i - discrete particle velocity
- c_i - lattice velocity (rescaled discrete particle velocity)
- c_s - sound velocity
- Ω - BGK collision operator.

- τ - relaxation time.
- τ_{f} - wall shear stress.
- τ_{s} - adhesive force per area.
- F_{f} - wall shear force.
- κ - erosion parameter. Details the toughness of the solid.
- m_0 - erosion parameter. Amount of mass contained in a solid node.
- ϕ_0 - erosion parameter. Van-der-Waals force value between two solid nodes which defines τ_{s}.

Chapter 2

Introduction

2.1 History of Erosion and Problem Description

Erosion is the process by which a solid body loses mass due to some interaction with a gas, liquid or solid. Aerosols generated by wind erosion is one of the largest sources of aerosols which affects the solar radiation absorption and reflection in the atmosphere [6]. Coastal erosion [7], which often gives rise to distinctive structures, e.g. the cliffs of Dover, see figure 2.1, is an example of where water slowly erodes away the shore. A study of solid-solid erosion of pebbles through collision with each other in a river has history dating back to the Greek philosophers [13]. Aristotle suggested that erosion causes the surface of the pebbles to be rounded. In particular, the points further away from the center of the pebble erode faster. This gives a nice explanation why rounded corners are a more common occurrence than sharp corners on pebbles in water. So it has been long known that erosion shapes the world around us and is studied in various fields. The pebbles that Aristotle studied today fall in the category of geological erosion. Here two typical problems are: (a) coastal erosion mentioned above. (b) how rivers change and erode the land around them [21].

Figure 2.1: Cliffs of Dover. Source information found here: [11].

The phenomenon is also studied in industrial fields. In the oil industry, erosion from sand particles in pipes can lead to the pipe breaking and causing environmental and economical damages [15]. While there are many different aspects to erosion, The type of erosion which we study here is erosion where a solid object in contact with a fluid loses mass to the fluid from the shear force the fluid applies on the solid. We will look at the implications it might have in the field of astrophysics.

Arguments have been made to suggest that erosion can determine the fate of planetesimals in proto-planetary disks [2] [17]. Planetesimals are potential starting points of planets formed from dust sticking together in a proto-planetary disk around a star according to the solar nebular disk model [3], which

contains the most widely accepted theories of planet formation. The model does however cover more generally the formation of stellar systems. There is no strict definition on a planetesimals size but can generally range in radius of cm up to km. The planetesimal and the gas in the disk moves at different speeds creating a headwind which allows for the erosion process to potentially happen. This is more closely described in section 6.4. While there exists theories on how planets form, it is not fully understood. Small planetesimals themselves are yet to be observed. Though their shape is thought to be similar to that of comets, spherical or two spheres stuck together, or, a snowman shape.

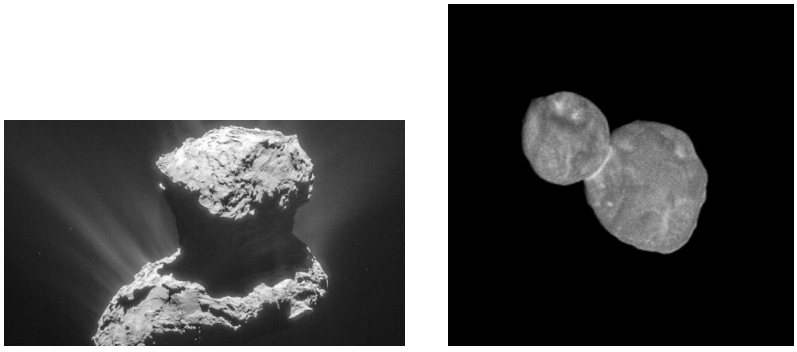

((a)) ((b))

Figure 2.2: (a): Rosetta comet [9], 27/05/2016. (b): Ultima Thule [16], 03/01/2019

The flow problem with erosion is a solution of the Navier-Stokes equation. This is a non-linear differential equation where very few solutions are known. The inclusion of boundary conditions which evaluates themselves based on the solution to the Navier-Stokes equation (moving boundaries) makes the problem even more difficult, both analytically and numerically. One way to help with the difficulty is to use an experimentally derived erosion model as a starting point [12] where the erosion rate is assumed and verified to be linearly proportional to the wall shear stress from the fluid [12]. We choose a model that is applicable to The types of objects with similar material properties to that of clay or mud-type objects, consisting of many small grains. Smaller planetesimals composition is theorized to be similar to that of clay or mud, many grains of dust sticking together. From this, equations characterizing the volume change due to erosion and estimates of the time it takes to completely erode in laminar flows and for a 3D sphere can be found. But for more physical scenarios where turbulence and more complicated objects than a sphere exists, numerical simulations must be used. To do this, and to solve the problem of moving boundaries, we develop a code based on Lattice-Boltzmann method (LBM). It is a fluid solver based on kinetic theory (the Boltzmann equation), unlike most other solvers which use continuum theory (Navier-Stokes equation) and it simulates weakly compressible flows. It has an advantage that the boundary conditions are implemented in such a way that moving boundaries become easy to deal with.

So the task is to build a numerical program using the Lattice-Boltzmann method to simulate erosion of 3 dimensional objects. In particular we study a sphere, a double sphere with different orientations and a cube. This is used to characterize the volume decrease and calculate the erosion time based on simulation results, derived equations and Reynolds number.

2.2 Overview of Thesis

We will first detail some kinetic theory background, including the Boltzmann equation and the Bhatnagar-Gross-Krook (BGK) collision operator. This will transition into a derivation of the Lattice-Boltzmann equations and define the boundary conditions used. Following this a verification of the flow

in the simulations in chapter 5 will be presented using the Poisseuille flow, some streamline figures and the Kolmogorov flow. This is to ensure that the flow in our simulations behaves correctly. Having established the framework for the LBM and verified the fluid flow, we in chapter 6 cover the theory of erosion, the numerical version of it and erosion of planetesimals. The experimentally derived model for erosion will be used as a starting point and from it, both the numerical equations and theoretical predictions will follow. A brief discussion of the erosion parameters will also be included. Before the results we will show how to go between physical units and LB units in chapter 7. Then the erosion results will be shown in chapter 8. Finally, a discussion on the results will be presented in chapter 9 where agreements and disagreements with experiments will be discussed. Conclusions based on the results obtained, possible improvements and future research will also be included. In the appendix one can find an overview of the structure of the algorithm and the code. The source code and video links will also be present in the appendix.

Chapter 3

Lattice-Boltzmann Theory

Fluid flows are often described using the Navier-Stokes equations which lies in the regime of continuum theory. Here one treats a fluid as a continuum, ignoring the fact that the fluid consists of smaller particles. But the Lattice-Boltzmann method lies in the regime of kinetic theory, where one instead looks at a fluid as a collection of many smaller particles. Of course, using Newton's equation of motion for all such particles when one usually has number of particles $>> 10^{23}$ is unrealistic. Instead one can use a statistical approach where one focuses on phase space distribution functions for the particles. If each particle were to have its own distribution function, the problem would again arise that there would be too many equations to solve. So under the assumption that each particle is indistinguishable in the fluid then for us there would only be necessary for a single particle distribution function f. The distribution function $f(\boldsymbol{x}, \boldsymbol{\xi}, t)$ gives the probability of finding a particle with position $\boldsymbol{x}$, velocity $\boldsymbol{\xi}$ and is the backbone of the LBM.

First the Boltzmann equation will be stated as it is equation from which the Lattice-Boltzmann equations are derived from. It will be simplified to the Boltzmann-BGK equation, and from there the full Lattice-Boltzmann equations will be derived. An equivalence between Lattice-Boltzmann and Navier-Stokes will be shown to provide central equations and show that Lattice-Boltzmann does indeed model the same type of dynamics as the NS equations given a few assumptions.

3.1 Theoretical Background

The Lattice-Boltzmann equations can be derived from the Boltzmann equation which is centered around the single-particle phase space distribution function $f(\boldsymbol{x}, \boldsymbol{\xi}, t)$.

$$\frac{df}{dt} = \frac{\partial f}{\partial t} + \boldsymbol{\xi}\frac{\partial f}{\partial \mathbf{x}} + \frac{\mathbf{F}}{\rho}\frac{\partial f}{\partial \boldsymbol{\xi}} = C(f). \tag{3.1}$$

Where $\frac{\partial f}{\partial t} + \boldsymbol{\xi}\frac{\partial f}{\partial \mathbf{x}}$ is the diffusion term, $\frac{\mathbf{F}}{\rho}\frac{\partial f}{\partial \boldsymbol{\xi}}$ is the force term and C(f) is the collision term. From it, all useful information about the system can be acquired. f is connected to macroscopic variables such as density, momentum, pressure/stress tensor, energy and heat flux through integration of f times some function of velocity $\boldsymbol{\xi}$.

$$\rho(\boldsymbol{x}, t) = \int f(\boldsymbol{x}, \boldsymbol{\xi}, t) d\boldsymbol{\xi}, \tag{3.2}$$

$$\boldsymbol{u}(\boldsymbol{x}, t) = \frac{1}{\rho}\int \boldsymbol{\xi} f(\boldsymbol{x}, \boldsymbol{\xi}, t) d\boldsymbol{\xi}, \tag{3.3}$$

$$\sigma(\boldsymbol{x}, t) = \int \boldsymbol{cc} f(\boldsymbol{x}, \boldsymbol{\xi}, t) d\boldsymbol{\xi}, \tag{3.4}$$

$$\epsilon(\boldsymbol{x},t) = \frac{1}{2\rho}\int \boldsymbol{c}^2 f(\boldsymbol{x},\boldsymbol{\xi},t)d\boldsymbol{\xi}, \tag{3.5}$$

$$\boldsymbol{q}(\boldsymbol{x},t) = \frac{1}{2}\int \boldsymbol{c}\boldsymbol{c}^2 f(\boldsymbol{x},\boldsymbol{\xi},t)d\boldsymbol{\xi}, \tag{3.6}$$

$\boldsymbol{c} = \boldsymbol{\xi} - \boldsymbol{u}$ is the mean velocity. The first 3 macroscopic variables will be the useful ones in our case and are the only ones which will be calculated in the simulation. All systems in this thesis will be isothermal.

The biggest problem when solving the Boltzmann equation is the complex collision operator $C(f)$ which describes the change in f after a two-particle collision assumed to be uncorrelated prior to collision.

$$C(f) = \int d^3\xi_1 \int d\Omega |\boldsymbol{\xi} - \boldsymbol{v_1}| \frac{\partial\sigma}{\partial\Omega}(f(\mathbf{p}')f(\mathbf{p_1'}) - f(\mathbf{p})f(\mathbf{p_1})). \tag{3.7}$$

To circumvent this problem, a simplified collision operator can be used, as long as it obeys some rules. The collision operator C(f) can be shown to have five collisional invariants [1] which satisfy

$$\int C(f) g_k(\boldsymbol{\xi}) d\boldsymbol{\xi} = 0, \qquad k = 1,2,3,4,5. \tag{3.8}$$

They are all different moments of velocity. $g_1 = 1, g_{2,3,4} = \boldsymbol{\xi}, g_5 = \boldsymbol{\xi}^2$. These five represent mass (g_1), momentum ($g_{2,3,4}$) and kinetic energy (g_5). The new collision operator must preserve these quantities. And it should also drive the distribution function f toward the Maxwell-Boltzmann distribution function according to the H-theorem [20]. The simplest collision operator obeying these rules is the BGK collision operator

$$\Omega(f) = -\frac{(f - f^{(\mathrm{eq})})}{\tau}. \tag{3.9}$$

Where $f^{(\mathrm{eq})}$ is chosen to be the Maxwell-Boltzmann equilibrium distribution function due to our systems following such statistics. τ is called a relaxation parameter which loosely determine how quickly the distribution evolves to equilibrium. It is connected to the viscosity (shown in 3.3) and is the parameter one mainly uses to change the Reynolds number due to its lower restrictions. One physical difference between $C(f)$ and $\Omega(f)$ is that the BGK collision operator predicts a different Prandtl number, which is the ratio between viscosity and thermal conduction. $C(f)$ predicts a Prandtl number value of $\approx 2/3$ which agrees with experiments of monatomic gases while $\Omega(f)$ predicts a value of 1. The expression for the equilibrium distribution function:

$$f^{(\mathrm{eq})} = \frac{\rho}{\sqrt{2\pi RT}} e^{-\frac{(\boldsymbol{\xi}-\boldsymbol{u})^2}{2RT}}. \tag{3.10}$$

$f^{(\mathrm{eq})}$ can be Taylor expanded to second order to give the expression

$$f^{(\mathrm{eq})} = \rho \frac{e^{-\frac{\boldsymbol{\xi}^2}{2c_\mathrm{s}^2}}}{c_\mathrm{s}\sqrt{2\pi}} \left(1 + \frac{\boldsymbol{\xi}\cdot\boldsymbol{u}}{c_\mathrm{s}^2} + \frac{(\boldsymbol{\xi}\cdot\boldsymbol{u})^2}{2c_\mathrm{s}^4} - \frac{\boldsymbol{u^2}}{2c_\mathrm{s}^2} + \mathcal{O}(\boldsymbol{u^3})\right). \tag{3.11}$$

The taylor expanded version is what will be used for the final equilibrium function expression. Motivation behind the expansion and its degree is given in chapter 3.2. The Taylor expansion of eq. (3.10) is valid in a low Mach-number regime, which is what the LBM simulations will be limited to. It is therefore of interest to know what the speed of sound is in the LB system. Sound speed is defined as

$$c_\mathrm{s} = \sqrt{\left(\frac{\partial p}{\partial \rho}\right)_S}. \tag{3.12}$$

The isothermal equation of state is defined as

$$p = \rho RT. \tag{3.13}$$

Putting (3.12) and (3.13) together,

$$c_\mathrm{s} = \sqrt{RT}. \tag{3.14}$$

Since the temperature is held constant, the sound speed will be a constant as well. c_s will then be assigned the value $\frac{1}{\sqrt{3}}$. This has to do with the Gauss-Hermite quadrature points in chapter 3.2 and will be shown there.

With $f^{(\mathrm{eq})}$ and $\Omega(f)$ defined, the Boltzmann equation can be re-written as the Boltzmann-BGK equation

$$\frac{\partial f}{\partial t} + \boldsymbol{\xi}\frac{\partial f}{\partial \boldsymbol{x}} = -\frac{f - f^{(\mathrm{eq})}}{\tau} - \frac{\boldsymbol{F}}{\rho}\frac{\partial f}{\partial \boldsymbol{\xi}}. \tag{3.15}$$

Where the left-hand side can be interpreted as the convection term and the right-hand side the collision plus force term. The force term will be used for the Poisseuille flow but put to zero for the following derivation results. It is used by adding a force term to the collision operator as the right hand side in equation 3.15.

3.2 Numerical Implementation

The equations we want to discretize in order to acquire the LBE is the macroscopic equations (3.2), (3.3), and the Boltzmann-BGK equation (3.15).

The first step is to discretize velocity space. The macroscopic variables in eq. (3.2) and (3.3) have to be calculated exactly in order to retain the fluid dynamics of the NS equation. An n:th order Gauss-Hermite quadrature will be a suitable choice for this, one of the reasons being that it can calculate polynomials with the form given in eq. (3.16) of order 2n - 1 exactly. According to the H-theorem mentioned earlier, The BGK collision operator will drive the distribution function f toward the equilibrium distribution function. $f^{(\mathrm{eq})}$ is an exponential function, but the Gauss-Hermite quadrature requires the function to be integrated over to have the form of

$$\int_{-\infty}^{+\infty} e^{-x^2} f(x)dx = \sum_{i=1}^{n} w_i f(x_i). \tag{3.16}$$

This can be solved by Taylor expanding $f^{(\mathrm{eq})}$ in $\boldsymbol{u}$, which motivates why it was done in eq. (3.11). Note that $\sqrt{RT}$ is substituted for c_s. It will eventually just become a constant but for clarity the sound speed is used for now. As for the order of the taylor expansion, second order is chosen because combined with the 3:rd order Gauss-Hermite quadrature it will calculate the macroscopic variables exactly. Given that the goal is to build a 3D simulation, f will depend on x,y,z, and 3:rd order quadrature will give 3 quadrature points in each x,y,z component (27 points total). This in LBM literature is called a D3Q27 model. The 3:rd order Gauss-Hermite quadrature is exact up to 5:th order polynomials. Looking at the macroscopic variables in eqs. (3.2) - (3.6), the distribution function is already multiplied by a 0:th-up to third-order polynomial. So Taylor expanding up to second order retains the exactness of the macroscopic variables given a 3:rd order quadrature. Other combinations of these orders exists, but will not be covered here since they won't be used.

Now the equilibrium function that needed to be integrated has the desired form with integration variable $\boldsymbol{\xi}$ and has a factor in front of it almost completely corresponding to the weights of a Hermite

polynomial. The macroscopic equations (3.2) and (3.3) becomes

$$\rho(\boldsymbol{x},t)=\sum_{i=1}^{27}f(\boldsymbol{x},\boldsymbol{\xi}_i,t) \tag{3.17}$$

$$\boldsymbol{u}(\boldsymbol{x},t)=\frac{1}{\rho}\sum_{i=1}^{27}\boldsymbol{\xi}_i f(\boldsymbol{x},\boldsymbol{\xi}_i,t) \tag{3.18}$$

To obtain the final form of $f^{(\mathrm{eq})}$, c_s needs to be determined. Recall from just below eq. (3.14) that $c_\mathrm{s}=\frac{1}{\sqrt{3}}$. The derivation will now follow.

$\frac{1}{\sqrt{3}}$ comes from that when $c_\mathrm{s}=\frac{1}{\sqrt{3}}$, the quadrature points will lie on an integer lattice [8]. Or in other words, ξ_i will be integer values (lattice vectors). And having integer lattice points for the lattice grid has a few advantages like makes unit conversions easier and computationally one only needs to store integers for lattice positions. When trying to determine the quadrature points such that they equal integer values, the value of c_s can be obtained.

The quadrature points are the roots to the n:th order Hermite polynomial $\mathcal{H}^n(\boldsymbol{\xi})$ defined by the weight function in D dimensional space $w(\boldsymbol{\xi})$ for $f^{(\mathrm{eq})}$. Here, D = 3 and n = 3.

$$w(\boldsymbol{\xi})=\frac{1}{c_\mathrm{s}\sqrt{2\pi}}e^{-\frac{\boldsymbol{\xi}^2}{2c_\mathrm{s}^2}},\qquad \mathcal{H}^n(\boldsymbol{\xi})=\frac{(-1)^n}{w(\boldsymbol{\xi})}\nabla^n w(\boldsymbol{\xi}). \tag{3.19}$$

For n = 3, this gives

$$\mathcal{H}^3(\boldsymbol{\xi})=-c_\mathrm{s}\sqrt{2\pi}e^{\frac{\boldsymbol{\xi}^2}{2c_\mathrm{s}^2}}\nabla^3\left(\frac{1}{c_\mathrm{s}\sqrt{2\pi}}e^{-\frac{\boldsymbol{\xi}^2}{2c_\mathrm{s}^2}}\right)= \tag{3.20}$$

$$=e^{\frac{\boldsymbol{\xi}^2}{2c_\mathrm{s}^2}}\left[e^{-\frac{\boldsymbol{\xi}^2}{2c_\mathrm{s}^2}}\left(\left(\frac{\boldsymbol{\xi}}{c_\mathrm{s}^2}\right)^3-2\frac{\boldsymbol{\xi}}{c_\mathrm{s}^4}-\frac{\boldsymbol{\xi}}{c_\mathrm{s}^4}\right)\right]=\frac{\boldsymbol{\xi}^3}{c_\mathrm{s}^6}-3\frac{\boldsymbol{\xi}}{c_\mathrm{s}^4}=0 \Rightarrow \tag{3.21}$$

$$\Rightarrow \boldsymbol{\xi}^3=3c_\mathrm{s}^2\boldsymbol{\xi}. \tag{3.22}$$

Eq. (3.22) have solutions $\xi_0=0,\xi_{\pm1}=\pm1$ if $c_\mathrm{s}^2=1/3 \Rightarrow c_\mathrm{s}=1/\sqrt{3}$. From this point on, ξ_i will be called c_i to denote that the discrete velocities are lattice vectors.

Using $c_\mathrm{s}=1/\sqrt{3}$ in eq. (3.11), the final expression for $f^{(\mathrm{eq})}$ becomes

$$f_i^{(\mathrm{eq})}=\rho w(c_i)\left(1+3(c_i\cdot\boldsymbol{u})+\frac{9}{2}(c_i\cdot\boldsymbol{u})^2-\frac{3}{2}\boldsymbol{u}^2\right). \tag{3.23}$$

The weights $w_i=w(c_i)$ can be derived from the definition of the weights in the Gauss-Hermite quadrature (n = 3)

$$w_i=\frac{2^{n-1}n!\sqrt{\pi}}{n^2[H_{n-1}(c_i)]^2}=\frac{24\sqrt{\pi}}{9(-9c_ic_i+3)^2}. \tag{3.24}$$

$$w_i=\left\{\begin{array}{ll}\frac{8}{27}, & i=0\\ \frac{2}{27}, & i=1,2,3,4,5,6\\ \frac{1}{54}, & i=7,8,...,17,18\\ \frac{1}{216}, & i=19,20,...,25,26\end{array}\right\} \tag{3.25}$$

w_i can also be found in [20], table 3.6. The factor $\sqrt{\pi}$ in eq. (3.24) can be normalized away since $\rho(\boldsymbol{u}=0)=\sum_i\rho w_i \Rightarrow \sum_i w_i=1$.

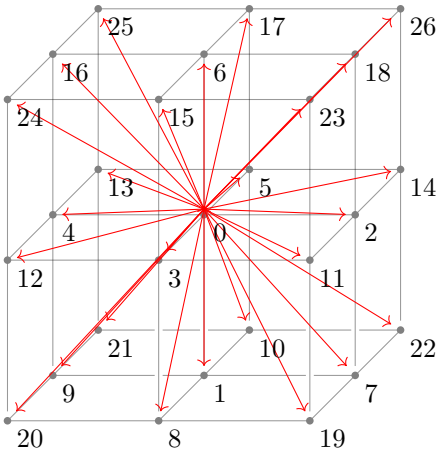

Figure 3.1: 3D visualization of the discretized distribution function f_i. The numbers at each node represents each index i.

Now that velocity space has been discretized through Gauss-Hermite quadrature, time and space has to be discretized as well. Setting the external force equal to zero (as mentioned earlier, it can later be taken into account through the collision operator), eq. (3.15) becomes

$$\frac{\partial f_i}{\partial t} = -c_i \frac{\partial f_i}{\partial \boldsymbol{x}} - \frac{f_i(\boldsymbol{x},t) - f_i^{(\mathrm{eq})}}{\tau}. \tag{3.26}$$

$f_i(\boldsymbol{x},t) = w_i f(\boldsymbol{x},\boldsymbol{\xi}_i,t)$. A first order forward Euler discretization can be used for the derivatives. It can be shown with the trapezoidal method [20] that while forward Euler is generally first order, here it will actually give second order accuracy.

$$\frac{f_i(\boldsymbol{x},t+\delta t) - f_i(\boldsymbol{x},t)}{\delta t} = -\xi_i \frac{f_i(\boldsymbol{x}+\delta x_i, t+\delta t) - f_i(\boldsymbol{x},t+\delta t)}{\delta x_i} - \frac{f_i(\boldsymbol{x},t) - f_i^{(\mathrm{eq})}}{\tau} = \tag{3.27}$$

$$= -c_i \frac{f_i(\boldsymbol{x}+c_i\delta t, t+\delta t) - f_i(\boldsymbol{x},t+\delta t)}{c_i \delta t} - \frac{f_i(\boldsymbol{x},t) - f_i^{(\mathrm{eq})}}{\tau}. \tag{3.28}$$

Rearranging terms to obtain the final form of the Lattice Boltzmann equations

$$\frac{f_i(\boldsymbol{x},t+\delta t) - f_i(\boldsymbol{x},t)}{\delta t} + \frac{f_i(\boldsymbol{x}+c_i\delta t, t+\delta t) - f_i(\boldsymbol{x},t+\delta t)}{\delta t} = -\frac{f_i(\boldsymbol{x},t) - f_i^{(\mathrm{eq})}}{\tau} => \tag{3.29}$$

$$=> f_i(\boldsymbol{x}+c_i\delta t, t+\delta t) = f_i(\boldsymbol{x},t) - \frac{\delta t}{\tau}\left(f_i(\boldsymbol{x},t) - f_i^{(\mathrm{eq})}\right) \tag{3.30}$$

This is the basic Lattice Boltzmann equation that will be used to to simulate the fluid dynamics through the distribution function f. The equation is usually divided into 2 separate parts, streaming step and collision step.

$$stream: \qquad f_i(\boldsymbol{x}+c_i\delta t, t) = f_i(\boldsymbol{x},t)$$

$$collision: \qquad f_i(\boldsymbol{x}+c_i\delta t, t+\delta t) = f_i(\boldsymbol{x}+c_i\delta t, t) - \frac{\delta t}{\tau}\left(f_i(\boldsymbol{x}+c_i\delta t, t) - f_i^{(\mathrm{eq})}\right)$$

These steps, along with the macroscopic variable equations (3.17) and (3.18), are the underlying equations to simulate fluid dynamics using the lattice Boltzmann method.

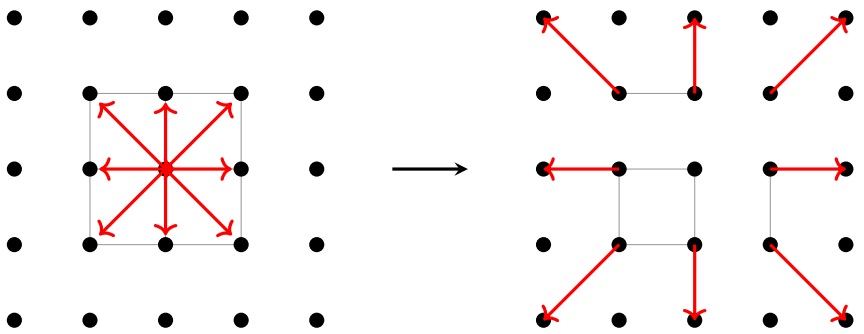

Figure 3.2: 2D illustration of the streaming step in LBM. A red arrow represents f_i for one momentum direction i. i = 0 does not move and remains at the center node.

3.3 From Lattice-Boltzmann to Navier-Stokes

The Navier-Stokes equation is the equation for modeling fluid dynamics, which is why most fluid solvers are based on it. However, the LBM is based on the Boltzmann-BGK equation (3.15). To ensure that the LBM replicates the behaviour of the Navier-Stokes equation, it is of interest to try and derive them from the Lattice Boltzmann equations. This will also show a core equation used in the simulations, namely the expression linking τ, the relaxation time, to the viscosity ν. An equation that can also be found through this derivation is the expression for the stress tensor which will be used later on, but will not be shown here due to an amount of algebra which made even the literature putting it in an appendix. This will be done using the Chapmann-Enskog expansion [20]. The idea is to do a perturbative expansion of f_i around $f_i^{(\mathrm{eq})}$ in terms of the Knudsen number ε. This will separate the physical properties of the density and momentum in different scales of the Knudsen number to eventually give rise to the Navier-Stokes continuity and momentum equations. This is also known as a multiscale expansion. Since the mass and momentum conservation are the ones taken into account in this thesis, those are the ones that will be derived from eq. (3.30). Let's start by stating the continuity and momentum equations from NS:

$$\left\{\begin{array}{l} \partial_t \rho + \partial_\alpha(\rho u_\alpha) = 0 \\ \partial_t(\rho u_\alpha) + \partial_\beta(\rho u_\alpha u_\beta) = -\partial_\alpha p + \partial_\beta\left[\mu\left(\partial_\beta u_\alpha + \partial_\alpha u_\beta\right) + \left(\mu_B - \frac{2\mu}{3}\right)\partial_\gamma u_\gamma \delta_{\alpha\beta}\right] \end{array}\right\} \tag{3.31}$$

$\partial_\alpha = \frac{\partial}{\partial x_\alpha}$. These are the ones the derivation will reproduce. Look at the lattice Boltzmann equation slightly reformulated

$$f_i(\boldsymbol{x} + c_i\delta t, t + \delta t) - f_i(\boldsymbol{x}, t) = -\frac{\delta t}{\tau}\left(f_i(\boldsymbol{x}, t) - f_i^{(\mathrm{eq})}\right) \tag{3.32}$$

The left-hand side is, again, the convection term. It can be Taylor expanded in the convection operator $(\partial_t + c_i\partial_\alpha)$

$$\delta t(\partial_t + c_i\partial_\alpha)f_i + \frac{\delta t^2}{2}(\partial_t + c_i\partial_\alpha)^2 f_i + \mathcal{O}(\delta t^3) = -\frac{\delta t}{\tau}\left(f_i - f_i^{(\mathrm{eq})}\right) \tag{3.33}$$

The expansion is made to to second order because the term $\delta t^n(\partial_t + c_i\partial_\alpha)^n f_i$ scales as $\mathcal{O}(\varepsilon^n)$ ([20], page 128). So the third orders and above will be small enough that they can be ignored. The labels of the f:s and ∂_t:s are used for the later recombination of the different scales of ε. To save time and effort, the second order derivatives of eq. (3.33) can be subtracted away by multiplying the equation

by $\frac{\delta t}{2}(\partial_t + c_i\partial_\alpha)$ and subtracting it from itself.

$$\delta t(\partial_t + c_i\partial_\alpha)f_i + \frac{\delta t^2}{2}(\partial_t + c_i\partial_\alpha)^2 f_i - \frac{\delta t}{2}(\partial_t + c_i\partial_\alpha)\left(\delta t(\partial_t + c_i\partial_\alpha)f_i + \frac{\delta t^2}{2}(\partial_t + c_i\partial_\alpha)^2 f_i\right) + \mathcal{O}(\delta t^3) = \tag{3.34}$$

$$= -\frac{\delta t}{\tau}\left(f_i - f_i^{(\mathrm{eq})}\right) + \frac{\delta t}{2}(\partial_t + c_i\partial_\alpha)\frac{\delta t}{\tau}\left(f_i - f_i^{(\mathrm{eq})}\right) => \tag{3.35}$$

$$=> \delta t(\partial_t + c_i\partial_\alpha)f_i = -\frac{\delta t}{\tau}\left(f_i - f_i^{(\mathrm{eq})}\right) + (\partial_t + c_i\partial_\alpha)\frac{\delta t^2}{2\tau}\left(f_i - f_i^{(\mathrm{eq})}\right). \tag{3.36}$$

Where the 3:rd order terms have been approximated away. Now, both f and ∂_t has to be expanded in ε:

$$\left\{\begin{matrix} f_i = f_i^{(0)} + \varepsilon f_i^{(1)} + \varepsilon^2 f_i^{(2)} + \mathcal{O}(\varepsilon^3) \\ \partial_t = \varepsilon\partial_t^{(1)} + \varepsilon^2\partial_t^{(2)} + \mathcal{O}(\varepsilon^3) \end{matrix}\right\} \tag{3.37}$$

Where $f^{(0)}$ is the equilibrium function but keeping the 0 for conventions sake. ∂_α does not need to be expanded but is labeled with (1) to remember the order of it. Solvability conditions will here be imposed as

$$\sum_i f_i^{(n)} = 0, \qquad \sum_i c_i f_i^{(n)} = 0, \qquad n = 1, 2, ... \tag{3.38}$$

These correspond to having the BGK collision operator preserving mass and momentum. They in turn give for the macroscopic equations 3.18 and 3.17:

$$\rho = \sum_i f_i^{(0)}, \qquad u = \frac{1}{\rho}\sum_i c_i f_i^{(0)}. \tag{3.39}$$

Continuing with inserting the expansions into eq. (3.36) and diving by δt:

$$\left(\varepsilon\partial_t^{(1)} + \varepsilon^2\partial_t^{(2)} + c_i\varepsilon\partial_\alpha^{(1)}\right)\left(f_i^{(0)} + \varepsilon f_i^{(1)} + \varepsilon^2 f_i^{(2)}\right) = \tag{3.40}$$

$$= \left(-\frac{1}{\tau} + \frac{\delta t}{\tau}(\varepsilon\partial_t^{(1)} + \varepsilon^2\partial_t^{(2)} + c_i\varepsilon\partial_\alpha^{(1)})\right)\left(f_i^{(0)} + \varepsilon f_i^{(1)} + \varepsilon^2 f_i^{(2)} - f_i^{(0)}\right) \tag{3.41}$$

Separating ε and ε^2, two equations pops out

$$(\partial_t^{(1)} + c_i\partial_\alpha^{(1)})f_i^{(0)} = -\frac{f_i^{(1)}}{\tau} \tag{3.42}$$

$$\partial_t^{(2)} f_i^{(0)} + (\partial_t^{(1)} + c_i\partial_\alpha^{(1)})f_i^{(1)} = -\frac{f_i^{(2)}}{\tau} + \frac{\delta t}{2\tau}(\partial_t^{(1)} + c_i\partial_\alpha^{(1)})f_i^{(1)} => \tag{3.43}$$

$$=> \partial_t^{(2)} f_i^{(0)} + \left(1 - \frac{\delta t}{2\tau}\right)(\partial_t^{(1)} + c_i\partial_\alpha^{(1)})f_i^{(1)} f_i^{(1)} = -\frac{f_i^{(2)}}{\tau} \tag{3.44}$$

Here some of the details of the derivation will be skipped due to it being very involved. But giving a short explanation of the following steps. Starting with equation (3.42) and multiplying it by 1, c_i, c_i^2 and summing up all the i components, one can find the Euler equations. The second order terms from equation (3.44) are required to derive the Navier-Stokes momentum equations. They can be seen as corrections to the first order equations. Multiplying them with 1 and c_i will give the continuity equation and the Navier-Stokes momentum equation. To obtain this final form, for this derivation, one must assume that $Ma << 1$ which again gives that the LBM method solves weakly compressible flows. The first time this is seen is in the Taylor expansion of the equilibrium distribution function. The Chapman-Enskog expansion of the Lattice-Boltzmann equations gives

$$\partial_t \rho + \partial_\gamma(\rho u_\gamma) = 0 \tag{3.45}$$

$$\partial_t(\rho u_\alpha) + \partial_\beta(\rho u_\alpha u_\beta) = -\partial_\alpha p + \partial_\beta \left[\rho c_s^2 \left(\tau - \frac{\delta t}{2}\right)(\partial_\beta u_\alpha + \partial_\alpha u_\beta)\right] \tag{3.46}$$

Comparing with equation (3.31), the continuity equation is the same and the momentum equation match if $\mu_b = \frac{2\mu}{3}$. This also produces the important equation used to link the relaxation time to the viscosity which is the equation most widely used in LBM to control the Reynolds number since velocity is limited by $Ma << 1$.

$$\mu = \rho c_s^2 \left(\tau - \frac{\delta t}{2}\right) = \rho\nu => \tag{3.47}$$

$$\nu = c_s^2 \left(\tau - \frac{\delta t}{2}\right) \tag{3.48}$$

δt is usually put to be equal to 1. Here one can see a restriction to the τ parameter. Viscosity can be defined as the amount of resistance a fluid has against being deformed. A negative value is then not typically allowed, so $\tau > 0.5$.

Chapter 4

Boundary Conditions

Boundary conditions at solid surfaces are necessary to describe how the fluid interacts with it. Here bounce back, or no slip, boundary conditions will be used. It corresponds to simulating a rough surface where the fluid velocity at the boundary is equal to zero. This is implemented with a simple rule. After streaming, at every boundary node position $\boldsymbol{x}_s$,

$$f_{i*}(\boldsymbol{x}_s, t + \delta t) = f_i(\boldsymbol{x}_s, t) \tag{4.1}$$

where $i*$ is the opposite direction of the incoming fluid density. Or in other words, $\xi_i = -\xi_{i*}$. This will effectively create a solid wall halfway between the fluid node and the boundary node as illustrated in the figure below.

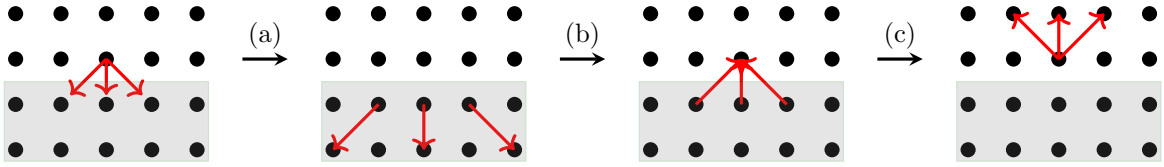

Figure 4.1: Bounce back sequence. (a) is the streaming step. (b) is the bounce back boundary condition. (c) is streaming step again. Grey area represents the solid domain while the white represents the fluid domain.

For Boundary conditions at the edges of the simulation box, Periodic and velocity boundary conditions are used. For the velocity boundary condition: The inlet will be managed by calculating the equilibrium distribution function corresponding to a chosen velocity u at ghost points outside the inlet direction. They will then stream into the the system. The outlet is dealt with by simply copying the distribution function to the outer set of ghost points. This works best for when the flow is not changing a lot at the outlet. But for our results it will provide sufficient accuracy as seen in the verification of the simulations.

Chapter 5

Flow Verification

To verify the flow of the LBM program, a good problem which has an analytical solution is the Poisseuille flow. It is an incompressible, laminar fluid flow in a straight 2D pipe (or a cylindrical pipe in 3D) with zero velocity at the boundaries (the no-slip boundary condition) driven by, for example, gravity. It produces a parabolic velocity profile for the flow with its maximum in the middle of the pipe. Solving the mass and momentum conservation equations, eq. (3.31), for the given boundary conditions and forces, one finds the velocity profile as

$$u(x) = \frac{\rho g}{2\mu}(a^2 - x^2) \tag{5.1}$$

where g is the gravitational constant, ρ is the density, μ is the dynamic viscosity, $2a$ is the width of the pipe and x is the position in the pipe. We compare the parabolic velocity profile to the velocity profile of the simulation in figure 5.1.

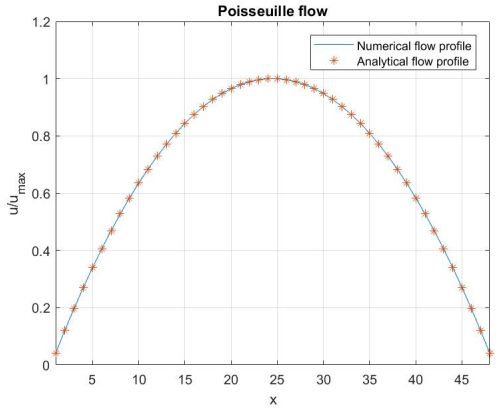

Figure 5.1: Comparison between simulation and analytical solution to the Poisseuille flow. Re = 30. Figure is taken as a snapshot at fixed y and z value. x shows position inside pipe. y axis shows velocity normalized by the maximum velocity.

Another verification is to look at the flow lines of a well-known fluid flow system. We can observe the flow lines for a laminar flow past a sphere and for turbulent flow past a sphere. Laminar flow, or creeping flow, is for low Reynolds numbers where the velocity of the flow is low, viscosity is high or the length scale of the cylinder is low. Turbulent flow is for high Reynolds numbers where the flow behind the cylinder (or the wake) becomes unstable and creates vortexes.

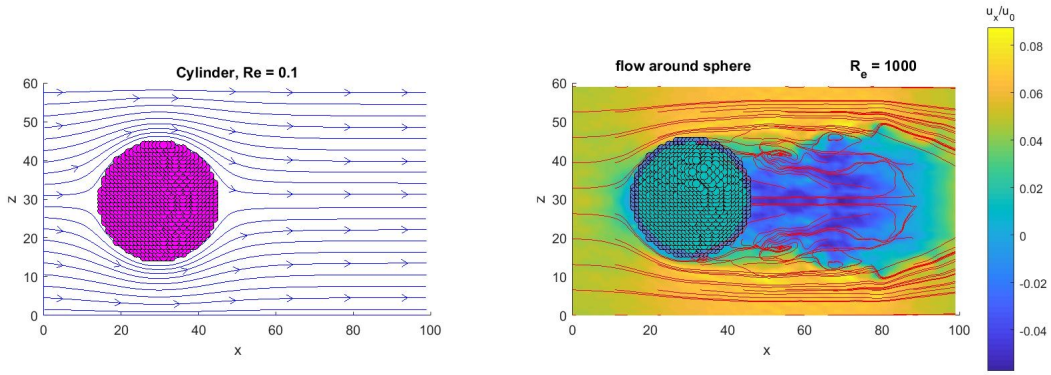

((a)) ((b))

Figure 5.2: Flow lines for different Reynolds numbers for (a) a cylinder and (b) a sphere. Inlet for both (a) and (b) is at x = 0. X and z values are grid positions.

A second type of flow is the Kolmogorov flow. It is an open flow driven by a cosinusodial force $F_{\mathrm{x}} = Acos(n\pi\frac{z}{z_{\mathrm{max}}})$ where A is just a constant and n is the amount of periods. The force is in x direction. For the laminar case, it should produce a flow profile similar to a cosine profile.

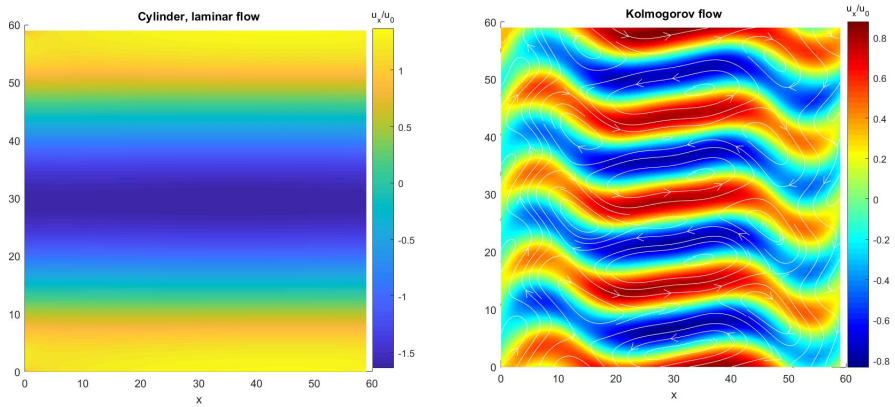

((a)) Laminar flow ((b)) Turbulent flow

Figure 5.3: We use an open flow without any solids (periodic boundary conditions in all directions) and drive the fluid with a force $F_x = cos(n\pi\frac{z}{Nz})$ where n is the amount of cosine waves put in. For the laminar flow, n = 1. For the turbulent flow, n = 8. X and z values are grid positions.

Chapter 6

Erosion

As stated in the introduction, erosion has been studied in many different fields before. But never in astrophysics. Given that small planetesimals are thought to be a collection of grains sticking together, the erosion of mudball-type objects which can loosely be defined as objects held together by many, much smaller grains will be used. It is assumed that the time it takes for the object to completely erode (the timescale for the erosion) is larger than the time it takes the fluid to pass the object since experiments show a large difference between the timescale of the erosion and the timescale of the fluid [18], [17]. The object is then also assumed to erode in a smooth, continuous fashion and not through big pieces relative to the object breaking off.

First the numerical aspects of the erosion calculation will take place. After that will follow a brief discussion on the parameters of the erosion equation. And lastly a derivation of the analytical predictions.

6.1 Model of erosion

The method of erosion is based on the work described in [12]. An experimentally derived and verified formula for the local erosion of an solid object is used.

$$\frac{dm}{dt} = \begin{Bmatrix} -\kappa(\tau_\mathrm{f} - \tau_\mathrm{s}), & \tau_\mathrm{f} > \tau_\mathrm{s} \\ 0, & \tau_\mathrm{f} < \tau_\mathrm{s} \end{Bmatrix} \tag{6.1}$$

where κ is the first erosion parameter and is related to the toughness of the solid object being eroded with units $[\frac{s}{m}]$, τ_f is the wall shear stress on the solid from the fluid in units of pressure and τ_s is a cutoff below which no erosion occurs. It can be though of as coming from the adhesive van-der-waals force keeping the solid surface together. $\dot{m}$ is calculated at every solid point and when the amount of mass loss equals a certain value m_0 (one of the erosion parameters), it gets removed. The wall shear stress is defined as

$$\tau_\mathrm{f} = \mu \frac{\partial u}{\partial x}\Big|_{x=0} \tag{6.2}$$

Where $\mu = \rho\nu$ is the dynamic viscosity, u is the velocity parallel to the surface and x is the distance from the surface. One can also identify the wall shear stress as the tangential component of the wall shear force F_f. To calculate τ_f in the LBM it is easier to calculate F_f and calculate the tangential part of it. This can be done using the deviatoric shear stress tensor, which is defined as

$$\sigma_{ab} = \mu \left(\frac{\partial u_a}{\partial x_b} + \frac{\partial u_b}{\partial x_a} \right). \tag{6.3}$$

σ_{ab} is by definition symmetric. It is a second degree tensor and can be interpreted as each column b contains the shear stress applied in a's direction. The equation in LBM for $F_{f,i}$ is

$$F_{fi}(\boldsymbol{x}) = \sum_{j=1}^{3} \hat{n}_j \sigma_{ij} = \sum_{j=1}^{3} \hat{n}_j \left(1 - \frac{1}{2\tau}\right) (f_q - f_q^{(\mathrm{eq})}) c_i c_j \tag{6.4}$$

Where the expression for σ, as mentioned in chapter 3.3, can be found from the Chapmann-Enskog expansion [20]. From this one can compute the tangential component, or τ_{f}, of F_{f} as

$$\tau_{\mathrm{f}} = \sqrt{(\hat{n} \cdot F_{\mathrm{f}})^2 - (\hat{n}(\hat{n} \cdot F_{\mathrm{f}}))^2}. \tag{6.5}$$

The estimate of the normal vector can be done by looking at the nearest neighbouring (NN) nodes. One sums up the lattice vectors from NN solid nodes and then normalize it.

$$\hat{n} = \frac{1}{a} \sum_{i=1}^{N} c_i \tag{6.6}$$

Where a is the normalization factor and i is the node index, not the component index of c. N is the number of NN solid nodes. In the code there is another step to this where after the nodes have been summed up, one transforms the vector to a lattice vector and then normalize. The advantage of this is that the square root does not have to be calculated for every normal vector since it will only ever be $\sqrt{3}, \sqrt{2}$ or 1 and the normal vector can be used for other parts of the code, saving memory space equal to a vector of size $3(N_x N_y N_z)^3$ where N_x, N_y, N_z is the dimensions of the simulation grid. The drawback of this is that for 2 rare types of positions on the grid, the numerical normal vector would point between two lattice nodes but is instead approximated to be the lattice vector closest to that vector.
F_s as stated earlier comes from the Van-der-Waals force. The reasoning for this is that surface forces will be the biggest contributor to counteracting the erosion. Nearest neighbour interaction for F_s is used due to the VDW force being a short-ranged force. F_s is calculated through setting the VDW force between two solid nodes as a parameter value ϕ_0 which is the second erosion parameter. Then summing up the contribution from all nearest neighbour solid nodes while taking distance into account.

$$F_s(\boldsymbol{x}) = \sum_{i=1}^{N} \phi_0 \boldsymbol{r}_i, \tag{6.7}$$

Where $\boldsymbol{r}_i$ is the distance from the node at $\boldsymbol{x}$ to the nearest neighbour node i (note that i is node index and not component index) and N is the total number of nearby solid nodes.

Now the fundamental erosion equations for the simulations have been presented. Some of the parameters deserve some discussion because some of them have proven difficult to find any reliable values for.

6.2 Estimates of Erosion Parameters

The κ parameter, which is related to the toughness of the solid, has never been measured directly for a planetesimal. However, comets might be objects similar to planetesimals. There have recently been some experimental data with information of the material that make up comets [10] from the Rosetta mission (landing on the Rosetta comet). This could be a possible way to experimentally estimate kappa. From [5], one estimate of kappa from experiments with soil erosion due to water flow gives $10^{-4} < \kappa < 10^{-3}$. They also emphasize the difficulty of calculating κ.

The m_0 parameter also needs some discussion. Looking at eq. (6.1), assume that the force is large enough to cause erosion. So for one timestep, an amount dm is being eroded away. How much mass is that in comparison to the sphere? a solid node won't be eroded away instantly, because that would defeat the purpose of even calculating dm. So how much mass is contained in a single solid node? Experimentally, it would be proportional to a small cube of solid matching the length scales of the grid in the simulation. But even then, a definition of the size of a grain of material from the solid would be required. To give a visual example, m_0 sort of says how many grains of material of the sphere exists in a single node. When dm reaches the value of m_0, the node is removed and eroded away from the sphere. This parameter was introduced into the simulations as a way of circumventing the fact that a discrete object is approximating a continuous one. m_0 is incorporated into a dimensionless number called the erosion number Er. Matching m_0 to a physical parameter has proven conceptually difficult but one idea is to absorb it into κ and have the numerical $\kappa_{numerical} = \kappa_{physical}/m_0$. This was at least used to compare the numerical t^* and theoretical t^* in figure 8.10.

Er is the dimensionless erosion parameter defined as $Er = \frac{\kappa}{m_0}(\tau_\mathrm{f} - \tau_\mathrm{s})\,\delta t$. It is a local quantity and contains information regarding how fast an object will erode. When Er = 1, a solid point erodes away. Let's say $\delta t = 1s$. If Er = 0.1 for a given node, then it will take 10 seconds for that node to erode. The maximum value for Er can then give an understanding as to how fast an object will erode, without having to worry about the exact values of κ and m_0. Calculating the corresponding physical mass for $1\delta x^3$, one could say how fast a part of the object would erode away and would help creating equivalent systems between simulations and experiments.

6.3 Analytical Theory of Erosion

The equations are based of the work from [18]. This will be an estimate for the volume change of a sphere due to erosion. And other constants will be used to estimate the time it takes for the body to erode completely. Let's restate the equation for clarity's sake.

$$\dot{m} = -\kappa(\tau_\mathrm{f} - \tau_\mathrm{s}). \tag{6.8}$$

Assuming that $\tau_\mathrm{f} >> \tau_\mathrm{s}$, using eq. (6.2) and approximating τ_f as $\mu\frac{U_0}{\delta(u,v)}$ where $\delta(u,v)$ is the boundary layer thickness at the surface point (u,v) and U_0 is the inlet velocity of the flow. Note that here we want a global expression for $\dot{M}$, M to denote the global aspect. Eq. (6.2) is a local one, so integration over the surface of the sphere is required.

$$\dot{M} \approx \int -\kappa\tau_\mathrm{f} \approx -\int \kappa\mu\frac{U_0}{\delta(u,v)}dudv = \tag{6.9}$$

u is the surface coordinate moving parallel to the flow. v is the surface coordinate moving perpendicular to the flow. the center of the coordinate system is placed at the stagnation point of the flow, or at the "front" of the sphere with respect to the flow direction. Since a sphere is used with no rotation, even with erosion there is a symmetry in the v direction. So the boundary layer thickness will only depend on the u coordinate. κ, μ and U_0 are all independent of u and v.

$$= -\kappa\mu U_0 \int_0^{L_u} \frac{1}{\delta(u)} \left(\int_0^{L_v(u)} dv \right) du = -\kappa\mu U_0 2\pi \int_0^{L_u} \frac{L_v(u)}{\delta(u)} du = \tag{6.10}$$

$\int dv$ will be an integration over a circle perpendicular to the flow around the sphere. $L_v(u)$ is a characteristic length (radius) of the integration circle given u. $L_u = 2R$, where R is the radius of the sphere, since we're assuming that we are working with a sphere and placing the origin of our coordinate system at the stagnation point of the flow on the sphere. Now we have to integrate the circle along the u direction. In a laminar flow, $\delta(u) \approx 4.91\sqrt{\frac{\nu u}{U_0}}$ [4].

$$= -\kappa\mu U_0 \int_0^{2R} \frac{L_v(u)}{4.91} \sqrt{\frac{U_0}{\nu u}} du = 4\pi\kappa\mu U_0^{3/2} \frac{1}{4.91\sqrt{\nu}} \int_0^{2R} \frac{L_v(u)}{\sqrt{u}} du. \tag{6.11}$$

$L_v(u)$ can be found through doing simple trigonometry:

$$R^2 = L_v(u)^2 - (R-u)^2 => L_v(u) = \sqrt{2Ru - u^2}. \tag{6.12}$$

This gives

$$\int_0^{2R} \frac{L_v(u)}{\sqrt{u}} du = \int_0^{2R} \sqrt{2R-u} du = \begin{pmatrix} x = 2R - u \\ -dx = du \\ u \to 0 => x \to 2R \\ u \to 2R => x \to 0 \end{pmatrix} = \tag{6.13}$$

$$-\int_{2R}^{0} \sqrt{x} dx = +\left[x^{3/2} \right]_0^{2R} = \sqrt{8} R^{3/2} = \sqrt{8}\sqrt{V} \tag{6.14}$$

where V is the volume of the sphere. Putting this back into eq. (6.11) gives

$$4\pi\kappa\mu U_0^{3/2} \frac{1}{4.91\sqrt{\nu}} \int_0^{2R} \frac{L_v(u)}{\sqrt{u}} du = 4\pi\kappa\mu U_0^{3/2} \frac{\sqrt{8}}{4.91\sqrt{\nu}} \sqrt{V}. \tag{6.15}$$

We can now find a separable differential equation for the volume:

$$\dot{M} = \rho\dot{V} = \frac{4\pi\sqrt{8}}{4.91\sqrt{\nu}} \kappa\mu U_0^{3/2} \sqrt{V} = \tag{6.16}$$

Solving this differential equation gives

$$\int_V^0 \frac{1}{\sqrt{V'}} dV' = \int_t^{t^*} \frac{4\pi\sqrt{8}}{4.91\sqrt{\nu}} \frac{\kappa\mu U_0^{3/2}}{\rho} dt' => 2\sqrt{V} = \frac{4\pi\sqrt{8}}{4.91} \kappa\sqrt{\nu} U_0^{3/2} (t^* - t) => \tag{6.17}$$

As one might have guessed, t^* is the time at which the sphere erodes away.

$$=> V = \left(\frac{4\pi\sqrt{8}}{2 \cdot 4.91} \kappa\sqrt{\nu} U_0^{3/2} t^* \right)^2 (1 - \frac{t}{t^*})^2. \tag{6.18}$$

From this, it seems that V should scale as $V \sim t^2$. In [18], their theory predicts that the area A scales as $A \sim t^{\frac{4}{3}}$ and confirm this theory with experiments. Using the relation that $V \sim A^{\frac{3}{2}}$, and inserting it into eq. (6.16), one can derive the relation $A \sim t^{\frac{4}{3}}$:

$$\rho\dot{A^{\frac{3}{2}}} = \rho A^{\frac{1}{2}}\dot{A} = \frac{4\pi\sqrt{8}}{4.91\sqrt{\nu}}\kappa\mu U_0^{3/2}A^{\frac{3}{4}} => A^{\frac{3}{4}} = \frac{4\pi\sqrt{8}}{4.91\sqrt{\nu}}\kappa\mu U_0^{3/2}(t^* - t) => \tag{6.19}$$

$$A = \left(\frac{4\pi\sqrt{8}}{2\cdot 4.91}\kappa\sqrt{\nu}U_0^{3/2}\right)^{\frac{4}{3}}(t^* - t)^{\frac{4}{3}}. \tag{6.20}$$

Back to the volume expression. Looking at the logarithm of the equation,

$$log(V) = 2log\left(\frac{4\pi\sqrt{8}}{2\cdot 4.91}\kappa\sqrt{\nu}U_0^{3/2}t^*\right) + 2log(1 - \frac{t}{t^*}). \tag{6.21}$$

It predicts a slope of two in a logarithmic scale for the erosion of a sphere. eq. (6.18) can also be reorganized to solve for t^*, the time at which the object erodes away. Doing the algebra, one finds

$$t^* = \frac{0.2763\cdot\sqrt{V_0}}{\sqrt{\nu}U_0^{3/2}\kappa}. \tag{6.22}$$

Do note that this is under the assumption of laminar flow (from the expression of the boundary layer) and for a sphere (the surface integration). But this can be tested against the simulations which can do turbulent flow and other shapes to see how well it matches.

6.4 Erosion in Proto-planetary Disk

Arguments supporting the notion that erosion could determine the fate of planetesimals is through a parameter study made by Noemi Schaffer at Lund University [2] and by wind tunnel experiments made by Paraskov, Wurm and Krauss [17]. The following arguments will be based on the work from [2].

The erosion of planetesimals comes from the fact that the planetesimal and the surrounding gas moves at different velocities. The gas moves at a sub-keplerian velocity due to a pressure gradient in the gas radially outward from the star [14]. And the planetesimal, while moving at keplerian velocity, can have an eccentric orbit which increases the velocity difference. This difference makes the planetesimal experience what is called a headwind that gives rise to a wall shear stress that potentially erodes it.

$$v_{\text{headwind}} = (e + \eta)v_{\text{kepler}} = (e + \eta)\sqrt{\frac{GM}{r}} \tag{6.23}$$

where G is the gravitational constant, M is the mass of the star, r is the radial distance from the star. η is the factor accounting for the velocity decrease from the pressure gradient and is taken to be $\eta = 10^{-3}$. e is the eccentricity of the orbit (elliptical deviation from circular orbit), where 0 is a circular orbit and $0 < e < 1$ is an elliptical orbit.

Paraskov, Wurm and Krauss have presented a theoretical estimate on the minimum amount of pressure required for erosion to occur on planetesimals in a proto-planetary disk. This lower limit of pressure they find to be $\sim$ 25Pa. Using the experimental model for erosion, eq. (6.1), and other factors, one can do a order of magnitude parameter estimate of the wall shear stress of the planetesimal and find that for certain parameters it exceeds the 25Pa limit.

Starting similar to chapter 6.3, we approximate the wall shear stress τ_{f} as

$$\tau_{\text{f}} = \mu\frac{U}{\delta(L)}. \tag{6.24}$$

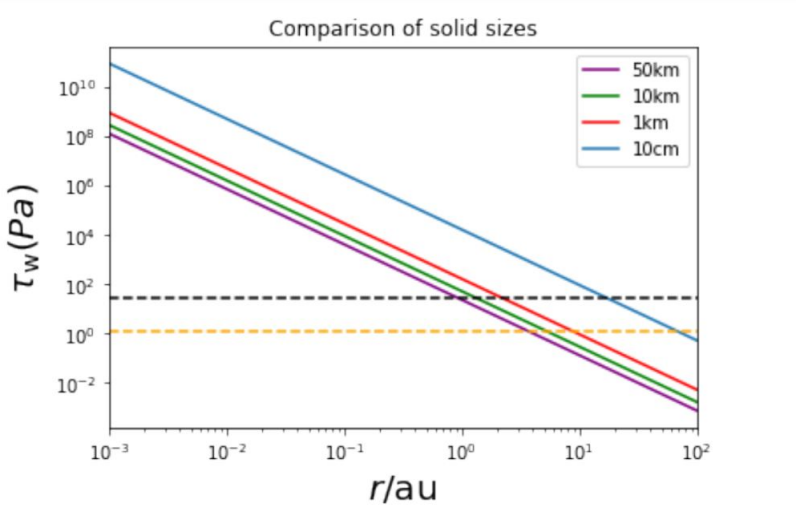

Figure 6.1: Wall shear stress of planetesimal vs its radius from the star. e is set to be 0.1. The 25Pa limit is represented by the black dashed line. The typical tensile strength of dust layers on comets with a typical porosity of 0.2 is 1.28Pa [19] and is represented by the orange dashed line.

Where U is the velocity, μ is the dynamic viscosity and $\delta(L)$ is the boundary layer thickness. Using earlier results,

$$\mu = \rho\nu, \qquad \delta(L) = \sqrt{\frac{\nu L}{U}}. \tag{6.25}$$

ρ is the density of the gas, ν is the kinematic viscosity of the gas and U is the relative velocity of the planetesimal with respect to the gas in the proto-planetary disk. With this, τ_f becomes

$$\tau_f = \rho\nu U\sqrt{\frac{U}{\nu L}} = \rho\nu^{1/2}L^{-1/2}U^{3/2} => \tag{6.26}$$

Using the fact that $Re = \frac{UL}{\nu}$:

$$=> \tau_f = \rho U^2 \frac{1}{Re^{1/2}}. \tag{6.27}$$

Values for these parameters can be found based on the radius L of the planetesimal, radius r from the star and the eccentricity e for their orbit. For example, a L = 1km solid body with eccentricity e = 0.1 would pass the the 25Pa limit at $r \approx 2.5au$.

Chapter 7

Units

The conversion from physical units to lattice Boltzmann units can be done in multiple ways. However, the core idea for the different methods is the same. The Reynolds number, a dimensionless quantity, should have the same value in both the simulation and in our physical system. If that is the case, and the geometry of the systems are the same, then the flow in our simulation is considered to be equivalent to the physical one. Two more parameters must also be in agreement, the erosion parameters (κ, m_0) mentioned in chapter 6.1. The erosion number could also be used.

The approach used here is to first go from physical units to dimensionless units by choosing an appropriate reference length, time and density and multiplying the physical units with these reference quantities to get non-dimensional numbers. From the dimensionless system, δx and δt can be used in a similar way to how the physical quantities were multiplied with the reference values to obtain the dimensionless numbers, the dimensionless numbers get multiplied with combinations of $\delta x, \delta t$ to obtain the system in lattice Boltzmann units.

Defining some variables:
l - length. u - velocity. t - time. ν - kinematic viscosity.
Physical units have lower notation p. Dimensionless units have lower notation d. And LB units will use the previously defined lattice step δx and time step δt.

The density can be chosen freely in the simulations and will thus be chosen as unity. It is necessary when converting things such as force or pressure. To get to dimensionless parameters, one can do dimensional analysis and use appropriate reference variables, in physical units, denoted with low index rp.

$$l_d = \frac{l_p}{l_{rp}}, \qquad t_d = \frac{t_p}{t_{rp}}, \qquad u_d = u_p \frac{t_{rp}}{l_{rp}} \qquad Re = \frac{l_r^2}{t_r \nu} \tag{7.1}$$

Reynolds number is already dimensionless and its expression stays the same in any form of units. But particularly, in a dimensionless system, where $l_{rd} = 1$ and $r_{rd} = 1$, $Re = \frac{1}{\nu_d}$. Examples of the reference variables: l_{rp} might be the length of the object in the flow. t_{rp} might be the time it takes the flow to pass the fluid. Whatever reference variables makes sense can be used here. From here the LB units can be defined.

$$l_{lb} = \delta x = \frac{l_{rd}}{N_l} = \frac{1}{N_l}, \qquad t_{lb} = \delta t = \frac{t_{rd}}{N_t} = \frac{1}{N_t}. \tag{7.2}$$

Where N_l is the number of points used to discretize the reference length l_r. The dimensionless transformation made it so that the reference time and length in dimensionless units will be equal to 1, hence

the 1 in the numerator. If the dimensionless step is skipped, these expression would be $\frac{l_{rp}}{N_l}$ and $\frac{t_{rp}}{N_t}$. And N_t is the number of time iterations it takes to reach the reference time t_r. Using these, the rest of the units can be found as well

$$u_{lb}\frac{\delta x}{\delta t} = u_d => u_{lb} = u_d\frac{\delta t}{\delta x}, \qquad \nu_{lb}\frac{\delta x^2}{\delta t} = \nu_d => \nu_{lb} = \frac{\delta t}{\delta x^2}\nu_d. \tag{7.3}$$

Variable	Physical Units $\rightarrow$	Dimensionless Units $\rightarrow$	LB units
length l	l_p	$\frac{l_p}{l_{rp}}$	$\frac{1}{N_l}$
time t	t_p	$\frac{t_p}{t_{rp}}$	$\frac{1}{N_t}$
velocity u	u_p	$u_p\frac{t_{rp}}{l_{rp}}$	$u_d\frac{\delta t}{\delta x}$
viscosity ν	ν_p	$\frac{1}{Re}$	$\nu_d\frac{\delta t}{\delta x^2}$

Table 7.1: Unit conversion for some variables. Note that for walking from physical units to LB units one can calculate the LB units with expressions mentioned in the explanation before this table, but the dimensionless step is adviced to do.

.

Chapter 8

Results

8.1 Comments on Figures

Snapshots of simulations shown in this chapter all have an inlet velocity at x = 0 and an outlet at x = x_{max}. For the general erosion results, conversion to physical units will not be necessary. But should one be curious, the methodology described in chapter 7 can be applied. Inlet velocity was set to $U_0 = 0.1$ and viscosity was changed in order to change Reynolds number. The different grid axes for the snapshots represent grid number.

8.2 Sphere

8.2.1 Re = 50

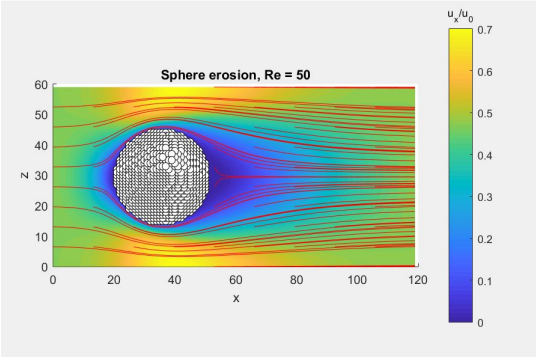

(a) $t/t_{pass} = 1$

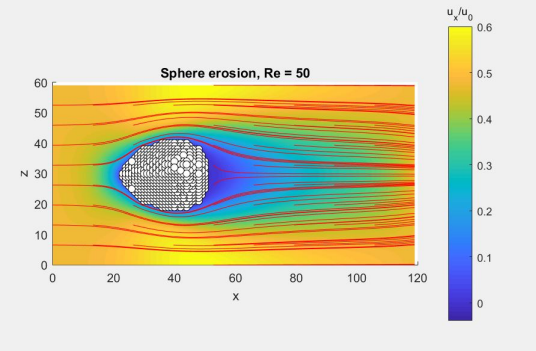

(b) $t/t_{pass} = 10$

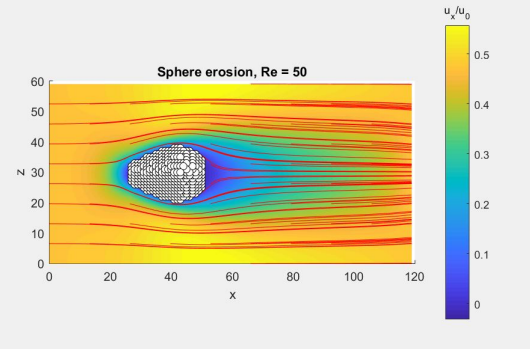

((c)) $t/t_{pass} = 16$

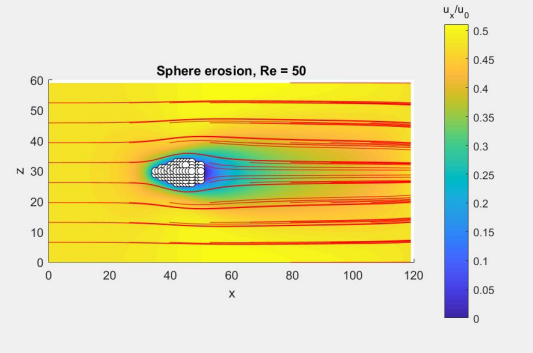

(d) $t/t_{pass} = 26$

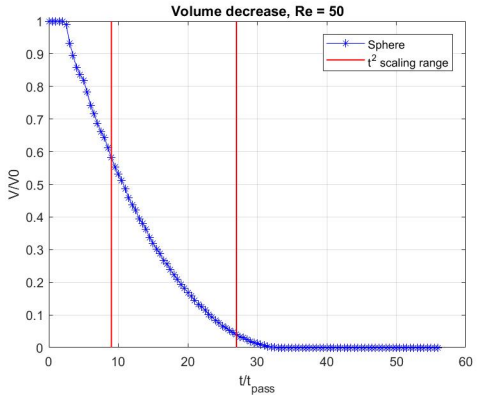

(e) Volume decrease for a sphere. x axis shows time in units of number of times the fluid has passed the sphere. and y axis shows the volume normalized by its initial value

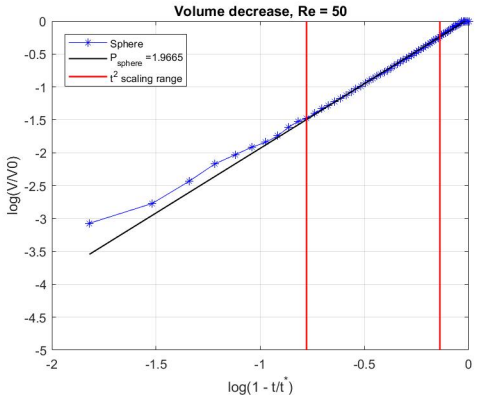

(f) Numerical calculation of the exponent of t in equation 6.18. Analytical value = 2. Numerical value = 1.966. The plot goes from right to left, from $log(1 - t/t^*) = 0$ to $log(1 - t/t^*) = -2$

Figure 8.1: Snapshots of erosion simulation at different times and showing corresponding volume over time graph and numerical power law exponent. t/t_{pass} represents the timescale scaled to number of times the fluid has passed the solid.

8.2.2 Re = 800

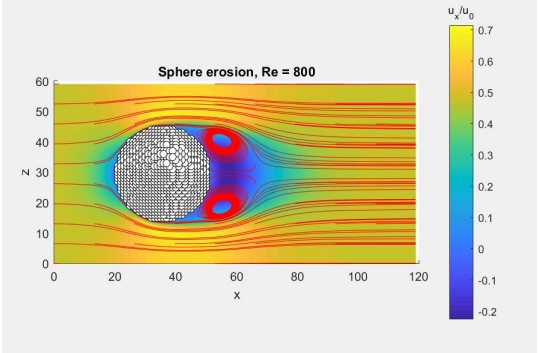

((a)) $t/t_{pass} = 1$

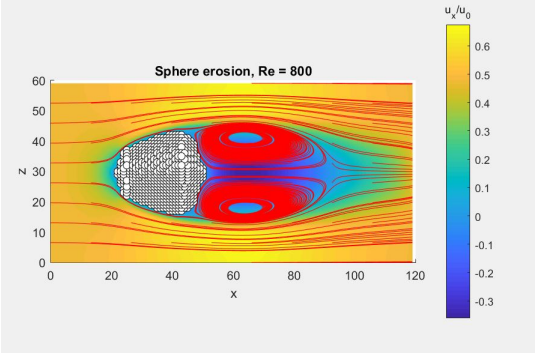

((b)) $t/t_{pass} = 8$

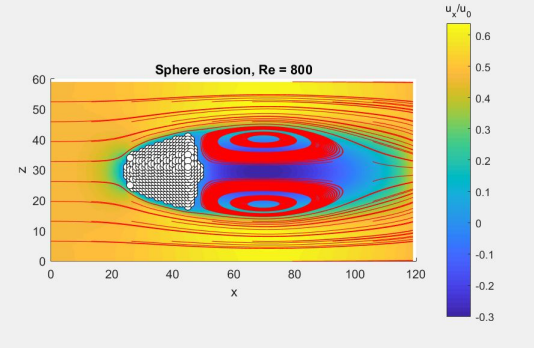

((c)) $t/t_{pass} = 16$

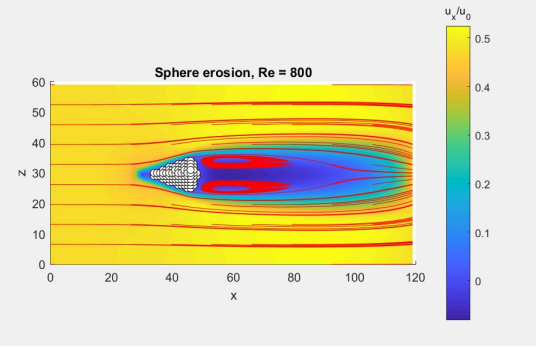

((d)) $t/t_{pass} = 30$

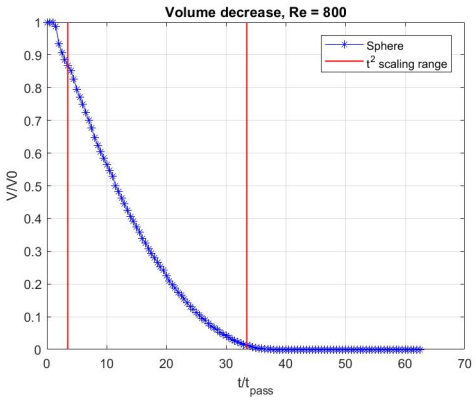

((e)) Volume decrease for a sphere. x axis shows time in units of number of times the fluid has passed the sphere. y axis shows the volume normalized by the initial volume.

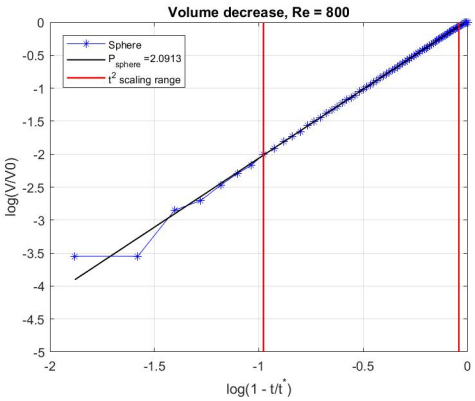

((f)) Numerical calculation of the exponent of t in equation 6.18. Analytical value = 2. Numerical value = 2.0913. The plot goes from right to left, from $log(1 - t/t^*) = 0$ to $log(1 - t/t^*) = -2$

Figure 8.2: Snapshots of a sphere in flow with Re = 800 and corresponding volume over time graph and numerical power law exponent. t/t_{pass} represents the timescale scaled to number of times the fluid has passed the solid.

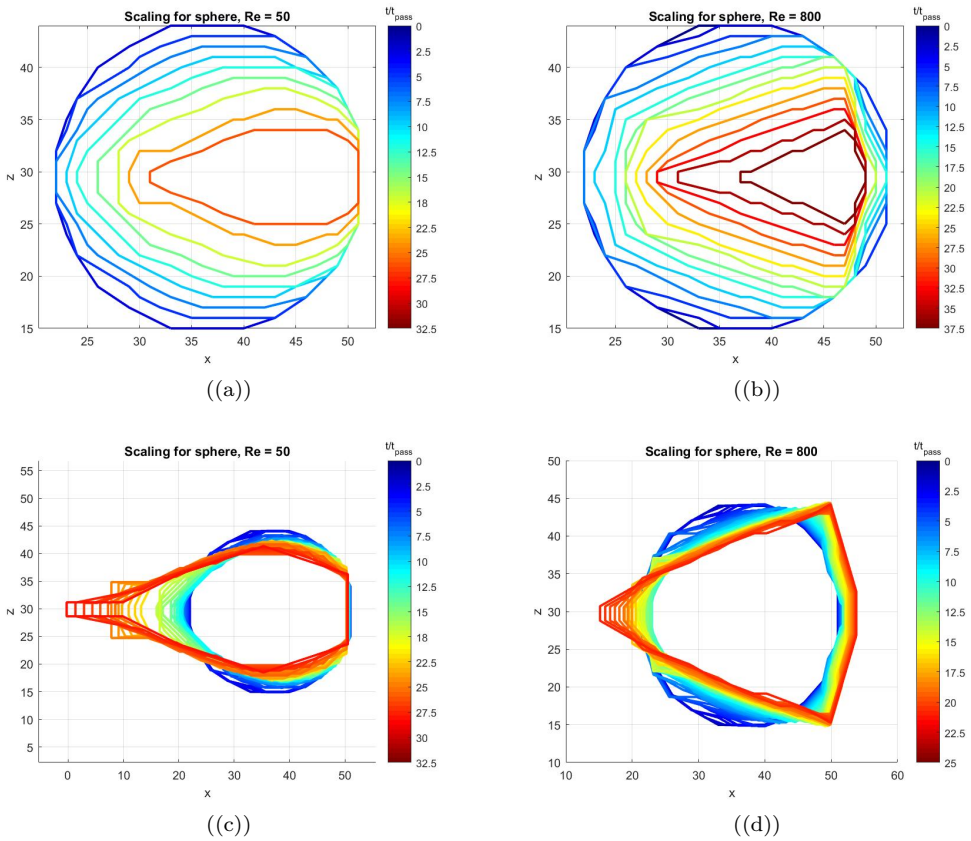

((a)) ((b)) ((c)) ((d))

Figure 8.3: Side Cross-section change over time due to erosion for a sphere. Time showed in (a) and (b) are from $t/t_{pass} = 0$ until the power law scaling can no longer be observed (when the volume becomes too small). (c) and (b) are (a) and (b) but cross-sections are normalized by their area.

The vortexes behind the sphere erode out concave surfaces in the sphere. Erosion is normally a process which forms convex shapes in this setup concave shapes can be formed from erosion.
The power law for the sphere seem to be in good agreement with experiments and analytical predictions for the power law which says that $V \sim t^2$. Numerical results show for Re $= 50$: $V \sim t^{1.96}$ in figure 8.1 and for Re $= 800$: $V \sim t^{2.09}$ in figure 8.2. The power law for the sphere in both Re $= 50$ and Re $= 800$ show that there are regions where the power law of t^2 is not very valid due to fluctuations or other trends.

Vague scaling can be seen in figure 8.3, (c) and (d), from $t/t_{pass} = 20$, $t/t_{pass} = 15$ and forward. For Re $= 50$, (c), the front of the sphere seemed to be more prone to discretization errors from its square shape unlike for Re $= 800$ (d), which show more clear scaling at later time. For lower Re a smoother shape seem to be favoured while at higher Re a wedge-like shape forms instead, creating sharp corners. The experiments in [18] show self-similarity arise later into the erosion experiment which would be consistent with the results presented here. They also observe a wedge-like shape forming after some erosion timescale.

8.3 Double Spheres and Cube

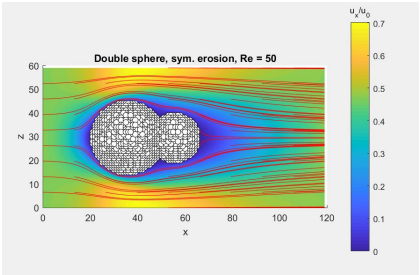

((a)) $t/t_{pass} = 1$

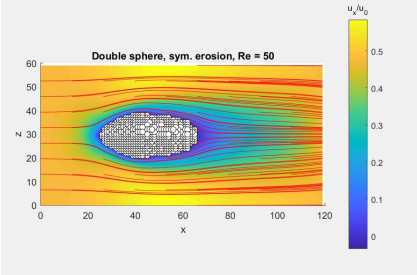

((b)) $t/t_{pass} = 16$

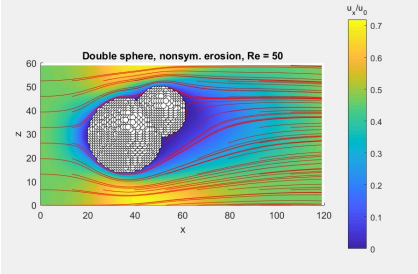

((c)) $t/t_{pass} = 1$

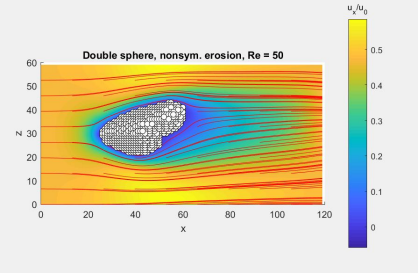

((d)) $t/t_{pass} = 18$

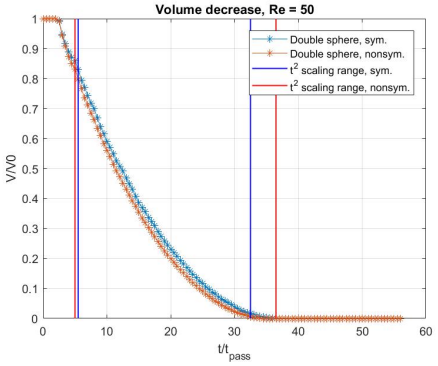

((e)) x axis shows the time in units of amount of times the fluid has passed the solid. y axis shows the volume normalized by the initial volume.

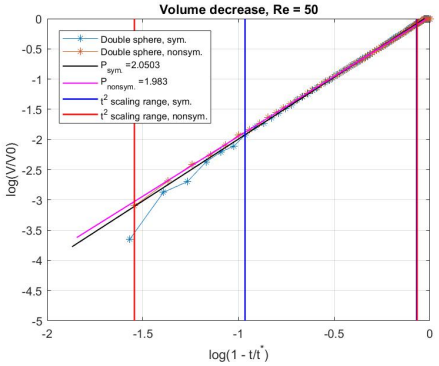

((f)) Power law for the double spheres at Re = 50. No analytical values exists. Figure reads from right to left. The vertical lines mark the area where the volume data follows a power law.

Figure 8.4: Snapshots from simulations, volume decrease and power law exponent for double spheres at Re = 50. t/t_{pass} represents the timescale scaled to number of times the fluid has passed the solid.

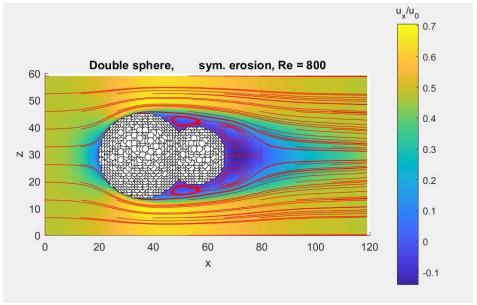

((a)) $t/t_{pass} = 1$

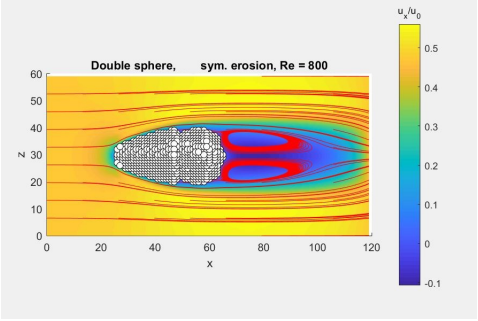

((b)) $t/t_{pass} = 22$

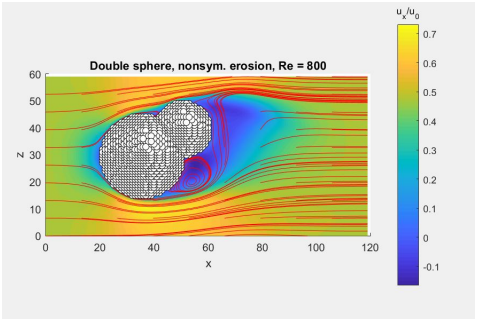

((c)) $t/t_{pass} = 1$

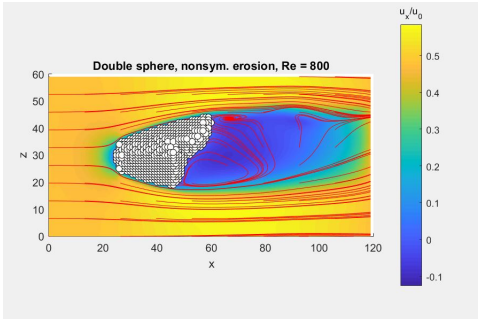

((d)) $t/t_{pass} = 18$

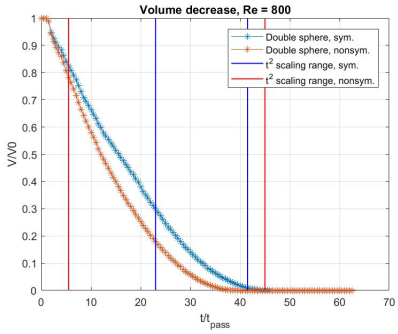

((e)) figure shows volume (normalized by the initial volume) decrease as a function of the time scale by amount of times the fluid passes the sphere.

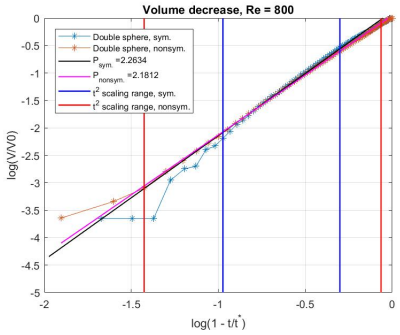

((f)) Power law for double sphere at Re = 800. figure reads from right to left. the vertical lines mark the area where the volume data follows a power law.

Figure 8.5: Snapshots from simulations, volume decrease and power law exponent for double spheres at Re = 800. t/t_{pass} represents the timescale scaled to number of times the fluid has passed the solid.

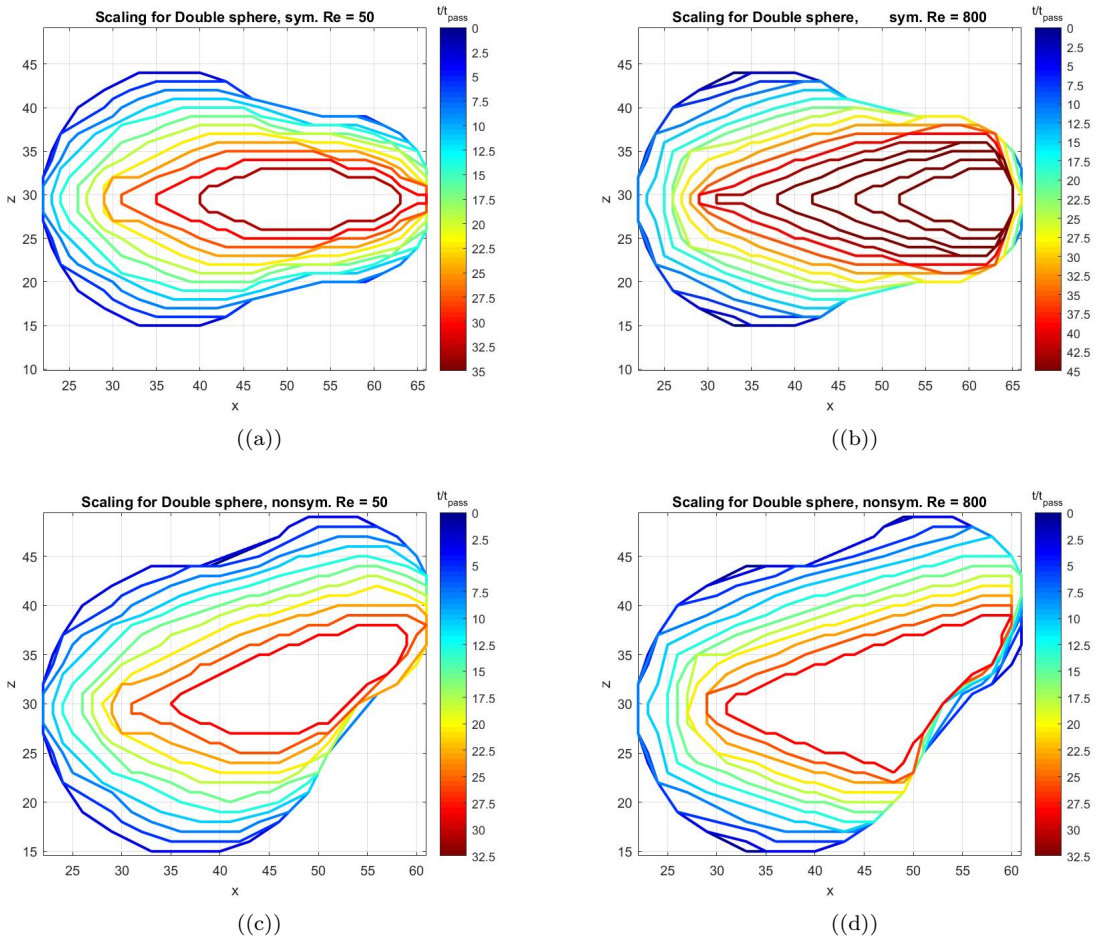

((a)) ((b))

((c)) ((d))

Figure 8.6: Double spheres were placed in a flow as in figure 8.4, 8.5 and snapshots of their xz-plane cross-section is shown in this figure at y = $y_{max}/2$.

The power law scaling for the double sphere has no analytical value but present theoretical framework seems to work for the double spheres. Figure 8.4, (a) and (b), Re = 50 show a power law exponent of 2.05 and 1.98. The similarity between the two spheres seem to deviate for Re = 800 where vortexes start to form, seen in figure 8.5. The power law region for the symmetrical double sphere shrinks and both power law exponents increase by $\sim +0.2$. So Reynolds number can have an effect on the power law behaviour.
The cross-section of the double spheres show a similar trait to the sphere, that erosion with Re = 50 produces a more smooth surface while Re = 800 can produce sharper corners and lines across the solid. Self-similar erosion is hard to gauge from the figures but some approximate similarity between the cross-sections can be seen.

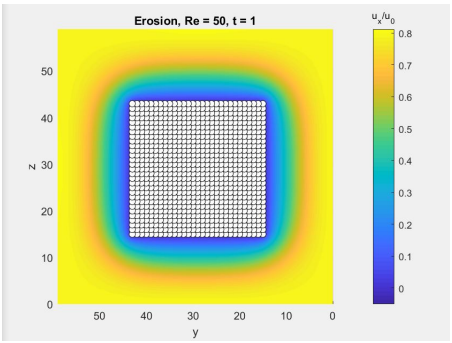

((a)) $t/t_{pass} = 1$

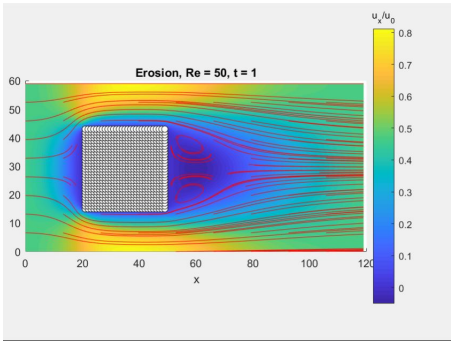

((b)) $t/t_{pass} = 1$

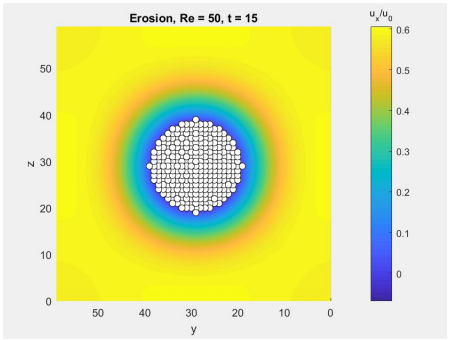

((c)) $t/t_{pass} = 30$

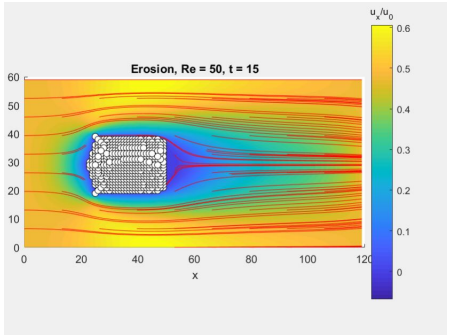

((d)) $t/t_{pass} = 30$

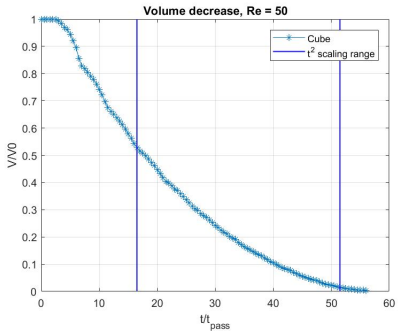

((e)) Volume as a function of time for a cube. x axis shows time and y axis shows the volume normalized by the initial volume.

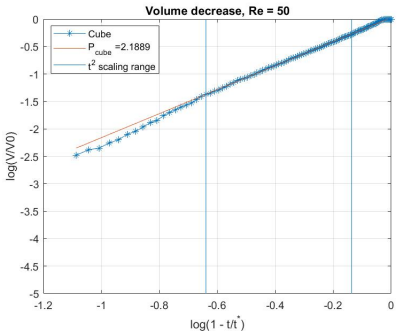

((f)) Power law exponent for a cube in Re = 50. The plot reads from right to left. Area where a power law can be seen is highlighted by the vertical lines.

Figure 8.7: Snapshots of erosion of a cube with corresponding volume graphs at Re = 50. Power law exponent = 2.1889. Some strange solid points/structures can be seen at the front of the cube after some erosion, possible due to numerical errors. t/t_{pass} represents the timescale scaled to number of times the fluid has passed the solid.

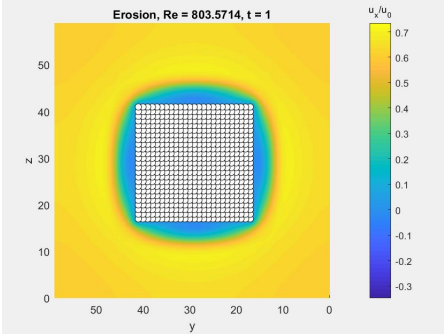

((a)) $t/t_{pass} = 1$

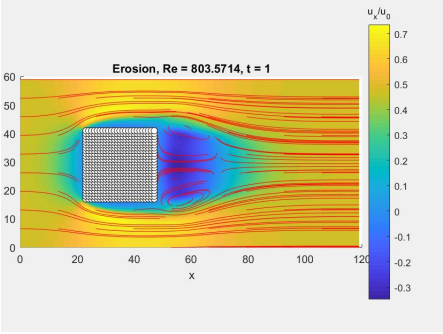

((b)) $t/t_{pass} = 1$

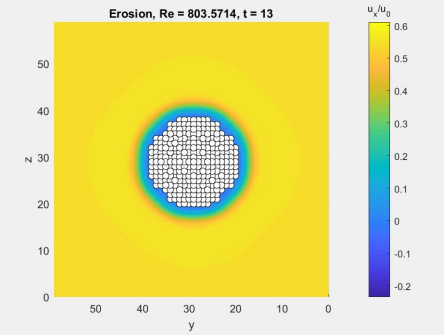

((c)) $t/t_{pass} = 16$

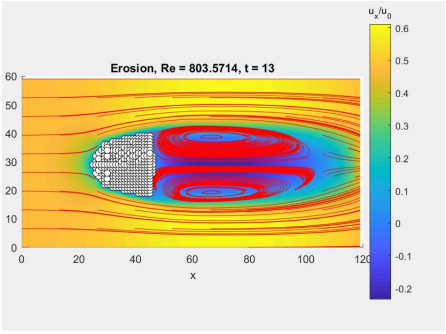

((d)) $t/t_{pass} = 16$

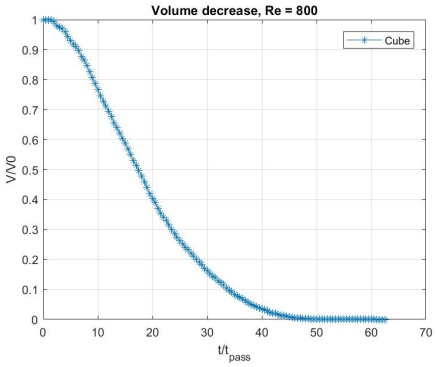

((e)) Volume as function of time for a cube. x axis shows the time and y axis shows the volume normalized by the initial volume.

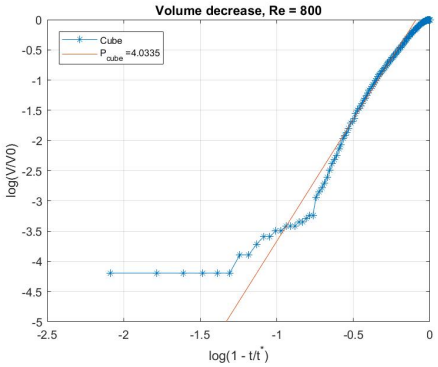

((f)) power law exponent for cube. The plot goes from right to left, from $log(1 - t/t^*) = 0$ to $log(1 - t/t^*) = -2$

Figure 8.8: Snapshots from erosion of a cube and corresponding volume change plots. t/t_{pass} represents the timescale scaled to number of times the fluid has passed the solid.

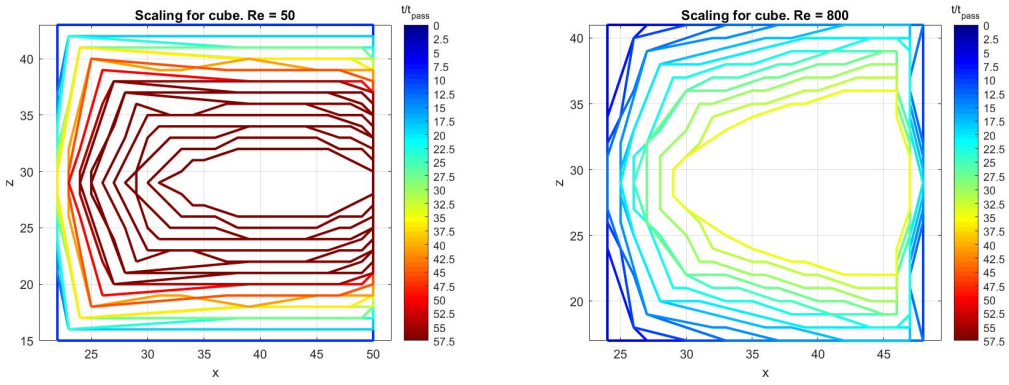

((a)) ((b))

Figure 8.9: A cube was placed in a flow and eroded with (a): Re = 50 and (b): Re = 800. During the simulations, we took snapshots of the xz-plane cross-sections and plotted them on top of each other.

Erosion of a cube in a flow at Re = 50, figure 8.7 shows the cube eroding to a cross-section in the yz-plane almost identical to the sphere. Its volume decrease can be described with a power law that is close to the sphere:s, $t^{2.1889}$. Erosion of a cube in a flow with Re = 800 causes the cube to tend toward a spherical cross-section again, seen in figure 8.8. The vortexes forming behind the object erodes the cube to form concave surfaces. The theoretical power law does not hold for the cube at Re = 800 and in fact there does not appear to be an obvious power law to the cube. The xz-plane cross-sections from figure 8.9 show that the cube at Re = 800 erodes toward a cross-section resembling the sphere.

8.4 Erosion Time t^*

Using parameters from [18], we can test eq. (6.22) to see to what degree it holds. The experimental value for $t^* \approx 2.5$ hours. Using given parameters, the theoretical value for t^* becomes

$$U_0 = 0.46\ m/s, \qquad \nu \approx 10^{-6}\ m^2/s \qquad R = 0.025\ m \qquad \kappa = 10^{-3}\ s/m => \tag{8.1}$$

$$=> t^* = 1.99 \text{ hours}. \tag{8.2}$$

Given that kappa can vary with a factor of 10, so can the calculated t^* value. But it seems that the model can calculate t^* sufficiently well.

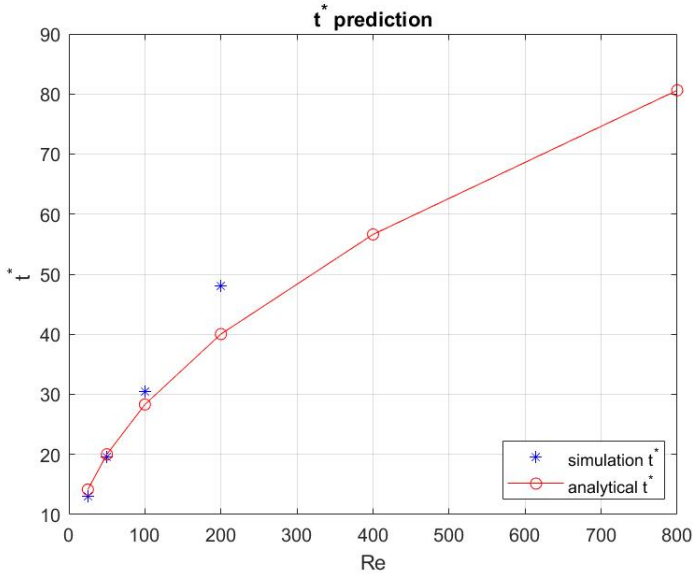

Figure 8.10: t^* calculated through eq. (6.22) and simulations. All values of t^* uses the same input parameters. $\kappa = 1$, $m_0 = 0.5$, $U_0 = 0.1$. Re was changed through changing ν. For Re $= 800$ but with $m_0 = 0.13$, numerical $t^* = 42$. Analytical $t^* = 20.4$.

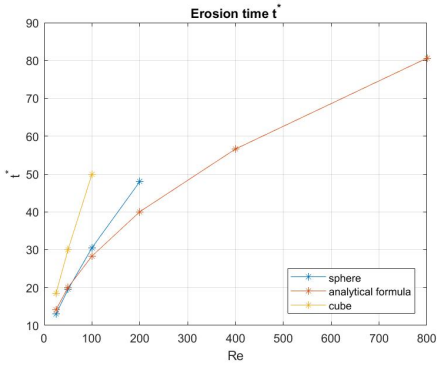

((a)) Estimates of erosion time t^* compared with analytical prediction. Cube and Sphere have the same initial volume.

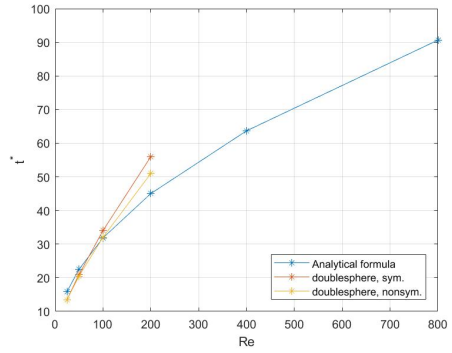

((b)) Estimates of erosion time t^* comapred with analytical prediction. The two double spheres have the same initial volume.

The erosion time estimate lies within a order of magnitude compared to the numerical calculations of t^* for Re $= 800$. The cube agrees less with the theoretical predictions. But seeing that the theoretical

formula for t^* holds within an order of magnitude for different shapes and non-laminar flow, eq. (6.22) can be used to give an order of magnitude estimate of the erosion time for planetesimals. Eq. (6.22) holds given that planetesimals can be modeled as cohesive soil, clay or a material of similar properties with a spherical shape and that $\tau_f >> \tau_s$ up to an order of magnitude. Using estimates from [14] for U_0 and ν and a value for κ from [5]:

$$U_0 = (\eta + e)v_{kepler} = (\eta + e)\sqrt{\frac{GM}{r}}\ m/s, \qquad \nu = c_s\lambda\ m^2/2 \tag{8.3}$$

$$\kappa \sim 10^{-3}\ s/m \tag{8.4}$$

where U_0 is the headwind (velocity difference between the planetesimal and surrounding gas in the proto-planetary disk). η is taken to be 10^{-3} from [14]. e is the eccentricity which is taken from [2] to ensure that $\tau_f >> \tau_s$ (the stress from the fluid is much larger than the critical threshold) at r = 1 a.u to allow erosion to occur. G is the gravitational constant. M is the solar mass. r is taken as 1 a.u. c_s is the sound speed at r = 1 a.u and scales with distance r as $\left(\frac{r}{au}\right)^{-1/4}$. λ is the mean free path of the gas in the disk set to 0.1m at r = 1 a.u. At r = 10 a.u λ increases to $\sim 10m$. The viscosity is for the gas in the disk. With these parameters, a planetesimal with radius R = 10cm and e = 0.013, and one with R = 1km and e = 0.1 would have erosion times of

$$t^*(R = 10cm, e = 0.013) \sim 10^{-4}s, \qquad t^*(R = 1km, e = 0.1) \sim 7.8s. \tag{8.5}$$

8.5 Erosion Number Scaling

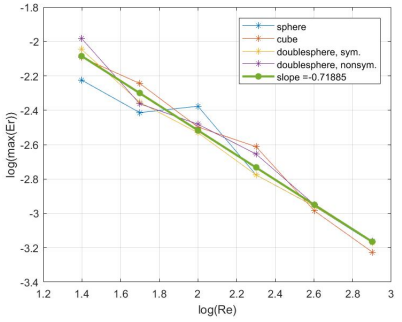

Figure 8.11: Maximum of the local erosion number for different Reynolds numbers. Erosion number was captured before erosion started.

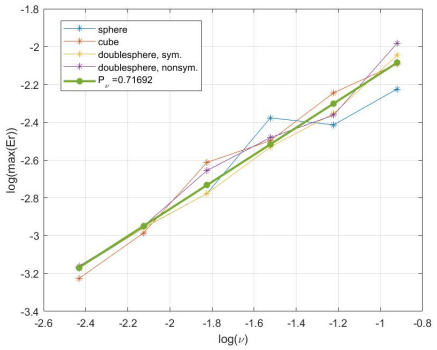

Figure 8.12: Relation between maximum local erosion number and ν. Erosion number was captured before erosion started.

The erosion number should theoretically scale with Reynolds number as $ErsimRe^{-0.5}$. The numerical value of $Er \sim Re^{-0.7}$ might be due to numerical errors or some flaw in the analytical calculation.

Chapter 9

Discussion

9.1 Erosion: Power Law and Scaling

The power law for V for the sphere shows good agreement with experiments for both Re = 50 and Re = 800 in figure 8.1 and 8.2. The power law deviates from the t^2 scaling in the beginning and the end of the plots, a characteristic seen for all shapes. The deviations at the end of all power law figures can most likely be explained by the fact that the solids are very small at that time ($V < 0.1 \cdot V_0$). And at some point, physically, a sphere small enough would just continue with the flow and not have a big velocity difference between it and the flow (less erosion). This is also the point where isolated points can start appearing in the simulation, which would also start following the flow since they become free from the main solid. That type of erosion would be different from the one being modeled through equation 6.1 since those isolated points don't follow the criteria that a certain mass has to have been eroded away from them in order to erode away. Numerically this difference should also be due to discretization errors. The deviation at the beginning of the plot might be due to numerical errors, but also might show that the erosion process doesn't follow the t^2 power law from the beginning.

The erosion plots for Re = 800 also show that the vortexes at the back of the sphere creates concave surfaces, something that was not observed in the experiments in [18]. This is probably due to the fact that they use turbulent flow and with the large difference between the flow timescale and the erosion timescale, these small erosion contributions from vortexes behind the sphere average out over time. While here the vortexes behind the sphere remain and erode out these concave surfaces. This was also observed for the cube with similar reasoning.

The cross-section plots of the sphere in figure 8.3 show at least for Re = 800 that the sphere does seem to after some time erode in a self-similar way. It cannot as clearly be concluded to be the case for Re = 50 due mostly to the front suffering from the low resolution of the sphere at that time. Re = 50 case does however seem to produce a more smooth shape while Re = 800 gives a sharper wedge shape. This behaviour can also be seen from [18] where the sphere erodes in a self-similar way later into the experiment and reaches a wedge with sharp corners (Re ¿ 800).

The double spheres showed almost exactly the same power law as the regular sphere from figure 8.4 and 8.5. This is rather surprising since at least for the non-symmetric double sphere, it does not posses the symmetry around the body in the direction perpendicular to the flow which is assumed in the derivation for the analytical expression for V. Perhaps the power law for erosion depends on things other than what is shown in the present analysis. One possible idea is that it might have to do with curvature. This possibility is however left as a possible future research topic and mentioned

below. The symmetric double sphere in Re = 800 did have a smaller region where the power law was visible, possible due to the vortexes forming in the cavity between the spheres. At t = 22 the cavity becomes too small to allow vortexes to form which coincides with where the power law region can be seen.

The erosion of a cube at Re = 50 seem to approximately follow the same power law as the sphere from figure 8.7. This similarity seems reasonable from the fact that the cross-section in the yz-plane which meets the flow is circular like the sphere. However, at Re = 800, figure 8.8 it does not appear to follow any power law. An approximate linear section was identified but not too much can be said from this. the cross-section snapshots reveal that it erodes to a very similar shape as the sphere in figure 8.2, which intuitively would lead to the argument that it should follow a similar erosion power law as the sphere. Unlike the other shapes it also seems that the beginning of the volume plot in figure 8.8 behaves more like a smooth curve rather than jumps into a t^2 power law. Again the vortexes at the back of the cube form concave surfaces.

The self-similarity property of the erosion was difficult to examine for the other shapes as it took a lot of time to produce the cross-section figure 8.3 for the sphere. One can see a tendency toward the shape changing less over time, but no concrete conclusions on that front can be drawn from them.

One difference between simulations and the experiments is that the difference between the timescale over which the erosion happens and the characteristic timescale of the fluid flow is much larger than the difference in the simulation. The choice for lowering this difference was because the results agreed with experiments anyway. And due to time restrictions, making the timescale difference match the experiments (while keeping a large enough size of the grid) would require a run time of over 6 months. So a timescale difference such that the volume power law sufficiently matched experimental data was chosen. One plan to circumvent this difference was to program the code to run in parallel on a GPU. This was originally intended to be included but was removed from the plan due to insufficient time.

9.2 Erosion Time t^*

The erosion time t^* for the different planetesimals is extremely low in astrophysical terms. Examining the method for arriving at t^*, there are three major assumptions we could examine.

First, we assumed that the force on the solid body is much larger than the cohesive force from the solid (by a factor of 10 given from the eccentricity used). This doesn't necessarily mean that the erosion has to happen fast if one has a low threshold and stress combined with a very low κ. But it might not be the case that this is true. If the stress is comparable to the threshold, it could greatly affect the erosion rate. So is $\tau_f >> \tau_s$ a reasonable assumption? The answer is probably. The stress from the fluid increases by increasing eccentricity which gives a behaviour where the headwind velocity increases from $U_0 = 24.38m/s$ for e = 0 to $U_0 = 268.2m/s$ for e = 0.013 which is a major increase for the force and contribution to the low t^*. So a low deviation from a circular orbit causes a large force increase which means that there is a much larger range of eccentricities for where $\tau_f >> \tau_s$ than when they are of comparable size. This can also be seen in [2].

The second assumption is that planetesimals can be considered to be made of material with similar properties to soil, clay or mud-type objects. If this is not the case then the model doesn't work and will produce nonsense. But since it is generally believed that planetesimals form by dust particles sticking together to form a larger mass, this assumption has some reasoning behind it.

Thirdly, the value for κ. It has already been stated that κ is difficult to determine and it depends strongly on material properties. But since the values of t^* are so low, it would take a change in κ from 10^{-3} to 10^{-13} to produce values on the order of 10^3 years. And even then a few thousand years is a

relatively short time span.

It might also be that the threshold for the erosion is higher than the value of 25Pa from [17]. But given that the model of erosion which eq. (6.22) for t^* is derived from is experimentally verified for soil or clay-type materials [12]. eq. (6.22) works within an order of magnitude even in turbulent flow and for different type of objects beside a sphere showed from the simulations which are themselves verified both analytically for the flow and experimentally for the erosion. eq. (6.22) can also reproduce a sensible value for κ as shown in 6.2. And even if κ or another parameter is wrong, t^* is so low that the erosion might still play a part in the growth of planetesimals.

This would then imply that low-eccentric orbits are favoured over high-eccentric orbits due to planetesimals in those high-eccentric orbits eroding away very rapidly. This is also the conclusion from [17].

9.3 Improvements

A more sophisticated method for the velocity boundary condition is the Zou & He velocity boundary condition [22]. The present method works better with higher grid resolutions and when there's low amount of change in the flow at the outlet but works sufficiently well for our considerations.

Extending the LBM code to run parallel on a GPU would have been one of the biggest improvements for the code. Lattice-Boltzmann gains a lot from being parallelized. Partially because it is "easy" (relative to other fluid solvers), and because of how the algorithm is structured. As mentioned earlier, it would allow us to run the code with a time difference between the fluid timescale and the erosion timescale matching natural erosion processes. And it would allow a better resolution of the solid objects possibly minimizing the resolution error preventing a nice self-similarity to be observed as in figure 8.3.

9.4 Future Research

One idea why the erosion for the double spheres seem to follow the same power law as the single sphere is due to their similar curvature. This would also explain why the cube deviated from the t^2 law at Re = 800. However, the cube at lower reynolds number showed a power law behaviour which might imply that Reynolds number matters and not just curvature. This is suggested as a possible future research topic and was briefly investigated by attempts at computing the curvature for the eroding sphere but was unsuccessful.

The arguments in chapter 6.3 can be made more general by not assuming a spherical shape, but rather a general shape. The calculations become more involved but do not lie in the realm of impossibilities. Possible general formula for how different shapes behave due to erosion (if they follow a power law, exponential, tangent function etc.) might come up from this.

The deposition of dust onto the planetesimal has not been included in the current framework and would be the counteracting force for the erosion. This can be implemented in the code and tested to see if there would be enough deposition to save the planetesimal for higher eccentric orbits.

Chapter 10

Conclusion

Erosion is a process which is important in many different fields. Coastal erosion in geology [7] and Aerosols generated by wind erosion [6]. It has been studied very little in astrophysics, particularly the erosion of planetesimals. A parameter study made at Lund university [2] and a wind tunnel experiment [17] has shown that erosion should affect the evolution of planetesimals. To do this we use a experimentally derived erosion model, eq. (6.1) which assumes the objects to be of a similar material to that of clay or soil. We use the model to develop a simulation code using the Lattice-Boltzmann method. Erosion is difficult to simulate due to the moving and shape-changing boundaries. The LBM is good at dealing with complex boundary conditions, which motivates the choice for it. We also derive a power law scaling for eroding spheres and a formula for the time it takes to erode an object. Since the time equation assumes laminar flow, and the power law is derived for a sphere, more complicated shapes and non-laminar flow is tested in the simulations. The flow in the simulations was verified by comparing flow profile with: a problem with existing analytical solution, the Poisseuille flow, the flow lines for various Reynolds number and the Kolmogorov flow. (figure 5.1, 5.2, 5.3).

Experiments and theoretical calculations based on the experimental model showed that a sphere's volume should erode according to the power law, $V \sim -t^2$. This was also seen in the simulations, figure 8.1, 8.2, where $V \sim -t^{1.96}$ for Re = 50 and $V \sim -t^{2.09}$ for Re = 800. The double sphere's and the cube at Re = 50 also followed a power law behaviour, figure 8.4, 8.5, 8.7, with approximately the same exponent as for the sphere ($P = 2 \pm 0.1$). The cube at Re = 800 did not follow a power law behaviour, figure 8.8.

The sphere seem to erode in a self-similar way after more than half its lifetime. Lower reynolds number produced a more smooth shape while higher produced sharper corners and slightly concave surfaces at the vortexes forming behind the sphere. Similar behaviour was seen for the other 3 objects.

The derived equation (6.22) for the erosion time t^* was based on laminar flow. But simulations showed that even in non-laminar flow, the equation still holds within an order of magnitude. A test-case showed that the equation could calculate the erosion time of a ball of clay eroding in water flow. The erosion time t^* for a planetesimal comes out to be very small, on the order of seconds. This is assuming an eccentricity of its orbit large enough to give that $\tau_f >> \tau_s$. So given that the estimate for the threshold of erosion to occur in planetesimals holds, then erosion should play a significant role for planetesimals evolution and indicates that orbits with very low eccentricity might be favoured.

Chapter 11

Appendix

11.1 Simulation Program

The simulation program is written in C++ using object-oriented programming and the visualization tools are written in MATLAB. The LBM code itself has 5 main files. One that deals with the basic LB steps (figure 11.2, steps 2,3,4,7,9). One that does the extra steps required for the erosion (figure 11.2, steps 5,6). One that contains all the input data. For example, outer boundary conditions, initial velocity etc. It mostly affects step 1 and 2 in figure 11.2. One that contains all the classes (definitions for all the vectors, solid objects, grid etc) and one that contains the main function.

11.2 Main Algorithm

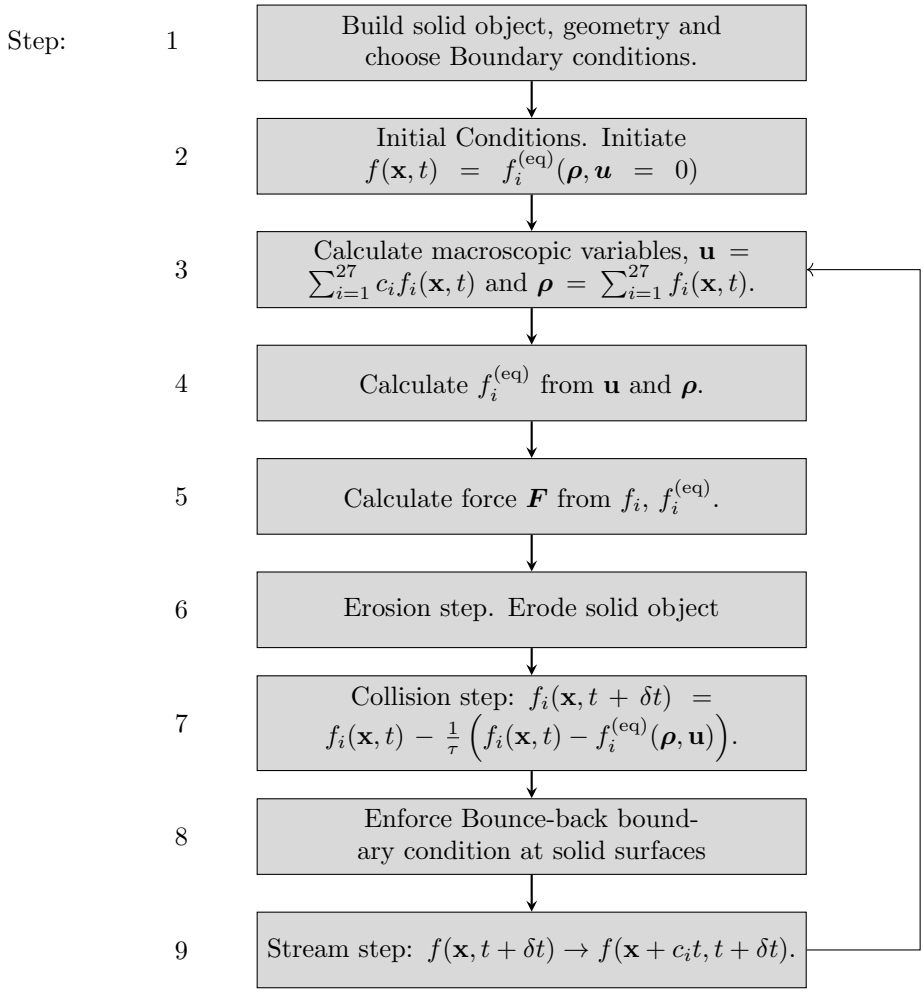

11.3 Step 1,2:

Here the solid object, inlet velocity, forces, geometry, κ, m_0, ϕ_0, τ, boundary conditions and some other parameters are chosen. The complete list can be found in the source code file LBM_input.cpp. Types of objects which have been implemented are: Sphere, Double sphere, Cylinder, Cube, Cylindrical pipe, Square pipe, 2D convex pipe and a triangle-wedge. Boundary conditions chosen here are the ones on the edges of the simulation box. This can either be periodic boundary conditions or velocity boundary condition. The boundary condition on the solid is only implemented as bounce-back. The distribution functions are also initialized as written in figure 11.2. A force applied to the fluid can also be chosen. Pre-programmed forces are gravity and a cosine force function used for the kolmogorov flow.

11.4 Step 3,4,7,8,9:

These parts handle the fluid dynamics. It uses two f_i distribution functions. function vector A is streamed and stored in function vector B. B is then used for the other various steps, for example,

calculating the macroscopic variables, the equilibrium distribution function etc. The function vector B collides and gets stored in A. And the cycle repeats. If streaming or collision happens first in the algorithm does not really matter. But the order of these 5 steps does.

11.5 Step 6: Erosion. Removing a solid node

The calculation for the erosion is described in chapter 6.1, but here will follow an explanation for how the deletion of a solid point is done. If a solid node was simply removed and the distributions left to fill the gap on their own, a small shock wave would be created since there are no distribution functions balancing the incoming ones from adjacent nodes to the one node removed. During the testing phase of the program, this developed instabilities which at times made the velocities diverge. And the erosion modeled is thought of to occur in a smooth fashion, which would mean that the fluid next to the eroding solid should not change abruptly due to the erosion process. So simply changing a point from solid to liquid might not work. But since the LBM works with discrete grids and points, some work-around has to be made. So when removing a point, of course the first step would be to change it to a liquid point. But the distribution function for the new liquid node must in the same step be populated by appropriate distribution functions to avoid the shock wave instability. And these distributions are chosen to be the the same as the interface node (fluid node closest to the solid node). This makes the flow change close to the surface sufficiently smooth and stable. The new surface nodes must also be populated with appropriate distribution functions to avoid another shock wave instability. These are chosen to be the new fluid nodes distribution functions by selectively streaming from the fluid node into the new surface nodes.

11.6 Source Code and Video Links

Source code can be found on github at:

https://github.com/Kakaboto/LBM3D.git.

Flow videos can be found on youtube at:

- Kolmogorov flow, unstable: https://www.youtube.com/watch?v=mUaoJcuvO4o
- Sphere flows:
  - https://www.youtube.com/watch?v=AbnxUVciUuo
  - https://www.youtube.com/watch?v=UKQiPr8-A14
  -
- Erosion of a symmetric double sphere in a flow:
  - Re = 50: https://www.youtube.com/watch?v=xXJFAkaoXxE
  - Re = 800: https://www.youtube.com/watch?v=QbHv618IxCw
- Erosion of a non-symmetric double sphere in a flow:
  - Re = 50: https://www.youtube.com/watch?v=prfAoSGqbow
  - Re = 800: https://www.youtube.com/watch?v=Ucnolpv4E3U
- Erosion of a cube in a flow, Re = 800:
  - Sideview: https://www.youtube.com/watch?v=xAFQJ-NqyYg&feature=youtu.be
  - Frontview: https://www.youtube.com/watch?v=q1EnoxZ_Ws0feature=youtu.be

Bibliography

[1] Penn State University Alberto Bressan Dept. of Mathematics. Notes on the boltzmann equation, 2005.

[2] Noemi Schaffer Lukas Cedenblad Anders Johansen, Dhrubaditya Mitra. Erosion of protoplanetary disk solids by gas flow. Unpublished paper, 2019.

[3] Philip J Armitage. *Astrophysics of planet formation*. Cambridge University Press, 2010.

[4] Cx K Batchelor and GK Batchelor. *An introduction to fluid dynamics*. Cambridge university press, 1967.

[5] Nadia Benahmed and Stéphane Bonelli. Internal erosion of cohesive soils: laboratory parametric study. In *6th International Conference on Scour and Erosion*, pages 8–p. SHF, 2012.

[6] WS Chepil. Dynamics of wind erosion: I. nature of movement of soil by wind. *Soil Science*, 60(4):305–320, 1945.

[7] Robin Davidson-Arnott. *Introduction to coastal processes and geomorphology*. Cambridge University Press, 2010.

[8] Paul J Dellar. Bulk and shear viscosities in lattice boltzmann equations. *Physical Review E*, 64(3):031203, 2001.

[9] 18-01-2019
European Space agency. https://www.esa.int/our_activities/space_science
/rosetta/rosetta_s_comet_contains_ingredients_for_life.

[10] Karl-Heinz Glassmeier, Hermann Boehnhardt, Detlef Koschny, Ekkehard Kührt, and Ingo Richter. The rosetta mission: flying towards the origin of the solar system. *Space Science Reviews*, 128(1-4):1–21, 2007.

[11] https://weather.com/science/environment/news/england-dover-cliffs erosion.

[12] Robin Jäger, Miller Mendoza, and Hans Jürgen Herrmann. Channelization in porous media driven by erosion and deposition. *Physical Review E*, 95(1):013110, 2017.

[13] Paul D Krynine. On the antiquity of "sedimentation" and hydrology (with some moral conclusions). *Geological Society of America Bulletin*, 71(11):1721–1726, 1960.

[14] Dhrubaditya Mitra, John S Wettlaufer, and Axel Brandenburg. Can planetesimals form by collisional fusion? *The Astrophysical Journal*, 773(2):120, 2013.

[15] T Montmerle, D Ehrenreich, A-M Lagrange, and AN Youdin. From grains to planetesimals. *European Astronomical Society Publications Series*, 41:187–207, 2010.

[16] 18-01-2019

NASA. http://pluto.jhuapl.edu/soc/ultimathule-encounter/.

[17] Georgi B Paraskov, Gerhard Wurm, and Oliver Krauss. Eolian erosion of dusty bodies in protoplanetary disks. *The Astrophysical Journal*, 648(2):1219, 2006.

[18] Leif Ristroph, Matthew NJ Moore, Stephen Childress, Michael J Shelley, and Jun Zhang. Sculpting of an erodible body by flowing water. *Proceedings of the National Academy of Sciences*, 109(48):19606–19609, 2012.

[19] Yuri Skorov and Jürgen Blum. Dust release and tensile strength of the non-volatile layer of cometary nuclei. *Icarus*, 221(1):1–11, 2012.

[20] Krüger Timm, H Kusumaatmaja, and A Kuzmin. *The lattice Boltzmann method: principles and practice*. Springer: Berlin, Germany, 2016.

[21] M. Coniglio L. Hardie V. Middleton, M. Church and F. Longstaffe. *Encyclopedia of Sediments and Sedimentary Rocks*. Springer: Neatherlands, 2005.

[22] Qisu Zou and Xiaoyi He. On pressure and velocity boundary conditions for the lattice boltzmann bgk model. *Physics of fluids*, 9(6):1591–1598, 1997.